CR-166426

NASA CONTRACTOR REPORT 166426

NEW CONSIDERATIONS ON SCALE EXTRAPOLATION OF WING PRESSURE DISTRIBUTIONS AFFECTED BY TRANSONIC SHOCK-INDUCED SEPARATION

Mohammad M. S. Khan
Jones F. Cahill

Contract NAS2-10855
October 1984

National Aeronautics and
Space Administration

NASA CONTRACTOR REPORT 166426

NEW CONSIDERATIONS ON SCALE EXTRAPOLATION OF WING PRESSURE DISTRIBUTIONS AFFECTED BY TRANSONIC SHOCK-INDUCED SEPARATION

Mohammad M. S. Khan
Jones F. Cahill
Lockheed-Georgia Co.

Contract NAS2-10855

National Aeronautics and
Space Administration

AMES RESEARCH CENTER
Moffett Field, California 94035

NASA CONTRACTOR REPORT 166426

NEW CONSIDERATIONS ON SCALE EXTRAPOLATION OF WING PRESSURE DISTRIBUTIONS AFFECTED BY TRANSONIC SHOCK-INDUCED SEPARATIONS

Part I. ANALYTICAL CONSIDERATIONS OF SHOCK-BOUNDARY LAYER CORRELATIONS - MOHAMMAD M. S. KHAN

Part II. REFINED EXTRAPOLATION OF WING LOAD DISTRIBUTIONS WITH TRANSONIC SHOCK-INDUCED SEPARATION - JONES F. CAHILL

PREPARED FOR:

NASA-AMES RESEARCH CENTER
BY THE LOCKHEED-GEORGIA COMPANY

PREFACE

NASA Contractor Report 3178 (published in 1979) presented a method for predicting the effects of change in Reynolds number on wing pressure distributions which are affected by transonic shock induced separations. That prediction was made possible by the discovery that the variation of trailing-edge pressure recovery with angle of attack and Mach number could be collapsed into a single curve through use of an empirically derived correlation parameter.

The information presented in this report consists of the results of studies identified as Tasks 2.1 and 2.2 of Contract NAS2-10855. These studies are concerned respectively with the derivation of an analytical parameter to replace the empirical parameter of CR3178, and with the refinement of the correlation process by use of the analytical parameter and other considerations.

This report is also identified as Lockheed Report LG83ER0055.

PART I. ANALYTICAL CONSIDERATIONS OF SHOCK BOUNDARY LAYER CORRELATIONS

Mohammad M. S. Khan

SUMMARY

Wing trailing-edge separations that occur at transonic speeds as a result of shock-boundary layer interactions are known to produce large adverse effects on aircraft aerodynamic characteristics. Large losses in lift and changes in wing torsional loads have been shown to result from such separations. Information on this subject for aircraft design must rely on wind tunnel test results. In currently existing wind tunnels, however, data can be obtained only at Reynolds numbers an order of magnitude less than flight values.

A procedure for extrapolating low Reynolds number pressure distribution data to flight conditions has been published in a previous NASA Contractor Report by Cahill and Connor. The correlation of trailing-edge separation data, which is vital to that extrapolation procedure, was developed purely from an empirical analysis of experimental data.

This report presents the results of a study that examines the basic fluid dynamic principles underlying shock-boundary layer interactions and develops an analytical parameter that should describe conditions leading to trailing-edge separation. The essential features of the interaction region are defined by using a triple-layer conceptualization of the controlling fluid dynamic phenomena. By matching conditions at the boundaries of the three layers, a parameter is derived that defines flow similarity in terms of susceptibility to separation downstream of the shock. It is concluded that a successful correlation of the separation data should include this similiarity parameter and a shape factor of the incoming boundary layer. Comparisons show a linear relationship between the similarity parameter developed here and the correlating parameter that successfully collapsed data on the development of trailing-edge separation in the previous work of Cahill and Connor.

NOMENCLATURE

$B1/2 = \dfrac{(P/P_s)\sqrt{M_\infty - A}}{\sqrt{1 - X_s/C}}$, empirical correlation parameter obtained by Cahill and Connor

C Airfoil Chord

C_f Wall friction coefficient

C_p Pressure coefficient

k vonKarman constant

$K = \dfrac{(M_e^2 - 1)}{(\gamma+1)\,\epsilon\, M_e^2}$ Similarity parameter

L Reference length

M Mach number

P Pressure

R_e Reynolds number

u Velocity parallel to the wall

u_τ Friction velocity

x Coordinate in streamwise direction

y Coordinate normal to the wall

γ Ratio of specific heats of air

δ Boundary layer thickness

$\delta+$ Wall layer thickness

ϵ Small perturbation parameter

μ Viscosity

ρ Density

τ_w Shear stress at wall

Superscripts

*	Dimensional quantities

Subscripts

0	Quantities related to incoming profile
e	Boundary layer edge quantities
s	Quantities at shock location

INTRODUCTION

The interaction of shock waves with boundary layers in transonic flows over wings is known to produce significant effects on the aerodynamics of high-speed aircraft. Local effects of the interaction include an increase in the displacement and momentum thickness, and a decrease in skin friction for some considerable distance, causing a possible separation of the boundary layer. Of greater importance is the modification introduced by the interaction to the boundary layer approaching the airfoil trailing edge that may change conditions for separation at the trailing edge. In such cases, the shock-wave boundary-layer interaction produces local as well as global effects represented by a loss in lift, increase in drag, and other adverse effects of separated flows, such as buffeting. Therefore, accurate prediction of shock boundary layer interaction and its effects on trailing-edge separation at flight conditions are critical for improved aircraft design.

Since the flow structure in shock-induced separation at transonic speeds is complex, the solution to the full Navier-Stokes equations must be considered for accurate prediction. Significant progress has been achieved in the development of methods for the direct numerical solution of the full Reynolds equation of turbulent flows. Although these methods hold the promise of offering the most complete and accurate solution for viscous flow, they have been limited in practice because of their large computing requirements. Experimental data obtained from wind tunnel testing are of great help to a designer in establishing a criterion for shock-induced trailing-edge separation. However, due to size limitations, much of the data are obtained at Reynolds numbers that are lower than flight condition Reynolds numbers. An effort to extrapolate wind tunnel data to flight conditions (Reynolds number and Mach number) has been

undertaken by Cahill and Conner (Ref. 1). Their correlation is based purely on an empirical analysis of experimental data. An extrapolation derived from consideration of fluid mechanics principles could be applied with much greater confidence.

The purpose of the present study is to develop analytical parameters that characterize the shock-wave boundary-layer interaction at transonic speeds. The intent is to illuminate the Cahill-Connor correlation and/or point to a more fundamental parameter for the interaction. Here we adopt an asymptotic analysis of the governing equations under conditions of incipient separation. This is because asymptotic solutions include the essential physics of the phenomenon of interaction as was demonstrated by Melnik and Grossman (refs. 2, 3) and Adamson, Liou, and Messiter (ref 4). In this report, we briefly describe the analyses and findings of these authors and then relate the basic parameters derived to those due to Cahill and Connor (ref. 1).

PROBLEM FORMULATION

Asymptotic Theory of Interaction

Several interrelated flow characteristics of the shock boundary-layer interaction region are shown in Figure 1. The incoming turbulent boundary-layer flow is slightly supersonic, except in a thin region near the wall where the flow is subsonic. The shock wave weakens as it penetrates into the boundary layer and terminates at the sonic line. Thus, the shock pressure-rise attenuates in the subsonic region beneath the shock, resulting in a smooth pressure distribution on the wall. It is clear that the pressure gradient normal to the wall in the interaction region is not small; hence, the classical boundary-layer formulation is inappropriate.

Melnik and Grossman (refs. 2, 3) considered a simplified model of a weak normal shock wave interaction with a fully developed turbulent boundary layer over a flat plate, as shown in Figure 2. The Reynolds number at the shock location is defined by

$$Re = U^*_e \rho^*_e L^* / \mu^*_e,$$

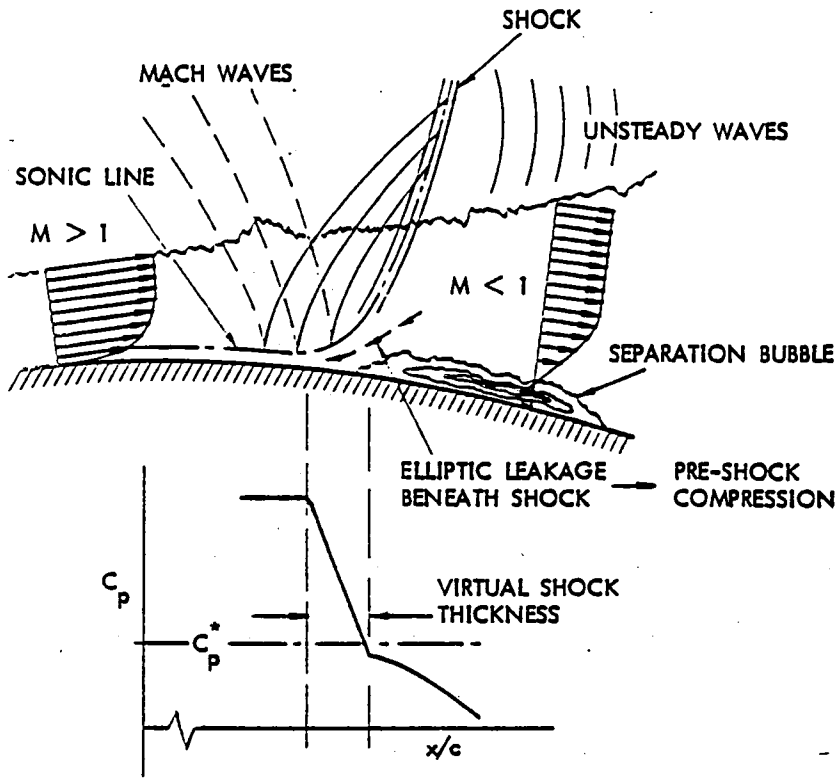

SURFACE PRESSURE DISTRIBUTION

FLOW UNSTEADY

INTERACTION COMPLEX

UPSTREAM INFLUENCE

SHOCK WEAKENS AS IT PENETRATES VELOCITY PROFILE

NOTE: $\frac{\partial P}{\partial y} \neq 0$ ⟶ B. L. APPROX. INVALID ⟶ δ^* CONCEPT INVALID

Figure 1. Flow Structure in the Shock/Boundary-Layer Interaction Region

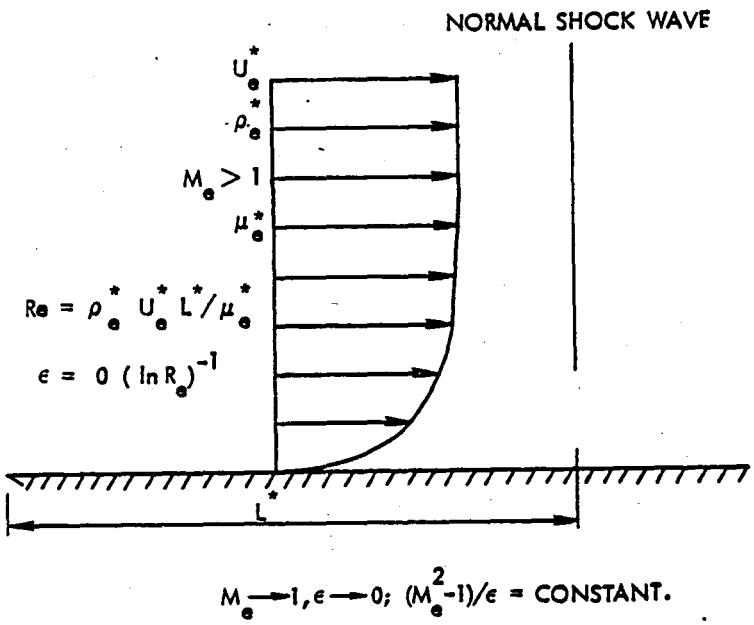

Figure 2. Melnik-Grossman Model of Weak Shock/Boundary-Layer Interaction

where U^*_e, ρ^*_e and μ^*_e are the undisturbed free-stream values of velocity, density, and viscosity, and L^* is the distance from the plate leading edge to the shock location. The wall shear stress and friction coefficient of the incoming boundary layer are related by

$$C_{f_o} = \tau^*_w / \frac{1}{2} \rho^*_e U^{*2}_e$$

A small parameter, defined by

$$\epsilon = (C_{f_o}/2)^{1/2} , \qquad (1)$$

is introduced, and we note that

$$\epsilon = 0 \left(\ell n \mathrm{Re} \right)^{-1} \tag{2}$$

thus $\epsilon \rightarrow 0$ as $\mathrm{Re} \rightarrow \infty$

The friction velocity is also given by $u_\tau = \epsilon U^*_e$. Let M_e denote the undisturbed Mach number. The analysis of Melnik and Grossman is based on a formal asymptotic expansion of the full Reynolds averaged Navier-Stokes equations in the double limit $M_e \rightarrow 1$ and $\epsilon \rightarrow 0$ (which implies $\mathrm{Re} \rightarrow \infty$) while $\chi \equiv (M_e^2 - 1) / \epsilon$ is held fixed. The parameter χ can be interpreted as a normalized shock strength because $(M_e^2 - 1)$ is the proportional to the shock strength and ϵ characterizes the "fullness" of the incoming velocity profile. The value of χ controls the relative rates at which the two basic parameters M_e and ϵ approach their respective limits. If the fixed value assigned to χ is O(1), then this limit is called "weak" shock limit.

Undisturbed Boundary Layer

Before considering the analysis in the interaction region, we review first the basic features of the asymptotic solution of the undisturbed compressible boundary layer over a flat plate in limit $R \rightarrow \infty$. The turbulent boundary layer at high Reynolds number develops a two-layer structure, as illustrated in Figure 3. In the outer region there is a balance between turbulent stress and convection of momentum. This region comprises most of the boundary layer, and the velocity profile is well represented by the small defect form of the law of the wake

$$U = 1 + \epsilon u_o \left(x, y/\delta \right) \tag{3}$$

where δ is the boundary layer thickness and x and y are cartesian axes, x is parallel, and y is normal to the plate. (Lengths and velocities are made dimensionless by using L^* and U_e^*, respectively). As a consequence of the

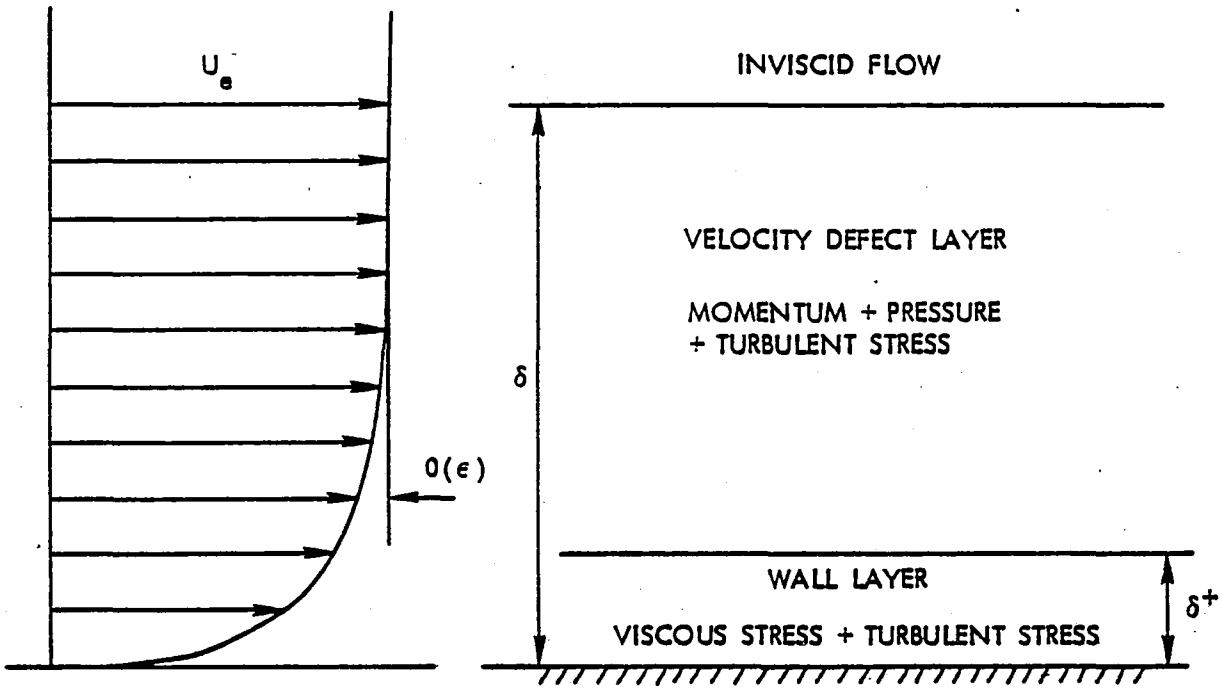

$$\epsilon = 0\ (\ln R_e)^{-1}\ ,\quad \delta = 0\ (\epsilon)$$
$$\delta^+ = 0\ [\ \epsilon^{-1}\ \mathrm{EXP}\ (-\tfrac{1}{\epsilon})\ ]$$

Figure 3. Schematic of the Undisturbed Boundary Layer

balance between the turbulent stress term and the convective terms in the x-momentum equation, we obtain the estimate

$$\delta = o(\epsilon) \tag{4}$$

In the inner region, in a very thin layer near the wall, there is a balance between turbulent and viscous stress while the convective terms are of smaller order of magnitude. The velocity profile takes on a law-of-the-wall form

$$U = \epsilon u_o(x, y/\delta^+) \tag{5}$$

where δ^+ is the thickness of the wall layer, and it is related to δ and Re by

$$\delta^+ = 0(Re\delta)^{-1} \tag{6}$$

In the overlap region, $y/\delta \ll 1 \ll y/\delta^+$, the velocity profiles in the outer and inner regions should match, and it follows from the matching that

$$\delta = 0(\epsilon) = 0\ (\ell nRe)^{-1} \tag{7}$$

and

$$\delta^+ = 0\ [\epsilon^{-1} \exp(-\epsilon^{-1})] \tag{8}$$

Equation (8) shows that, for high Reynolds number flows ($\epsilon \to o$), the wall layer is exponentially thin compared with the overall thickness of the boundary layer. From the matching of the velocity profiles it is also established that the profile has a logarithmic form in the overlap region,

$$U \to 1 + k^{-1}\epsilon\, \ell n\ (y/\delta) + \ldots, \text{ as } (y/\delta) \to o$$

and

$$U \to \epsilon[k^{-1}\, \ell n(y/\delta^+) + c] \quad , \text{ as } (y/\delta^+) \to \infty$$

with k = 0.41, the von Karman constant and c = 5.0. Therefore, the velocity profile in the defect layer does not satisfy the no-slip condition on the surface.

Finally, we notice that the pressure gradient, dp/dx, does not affect the wall layer unless it is $O[\epsilon^3 \text{ Exp } (\epsilon^{-1})]$. This follows from equating the order of dp/dx to that of the viscous stress term in the x-momentum equation.

Interaction Region

Upstream of the interaction region, the boundary layer has a two-layer, law of the wake/law of the wall, form. Outside the boundary layer there is an inviscid, irrotational flow that contains a weak normal shock wave. In the interaction region, sketched in Figure 4, the boundary layer develops a three-layer structure. The extent of the interaction region in the streamwise direction is $O(\epsilon^{3/2})$, and it is the same for the three layers. The main deck has a thickness $O(\epsilon)$ and thus extends over most of the boundary layer. Because the streamwise extent of the interaction is small in comparison with the boundary-layer thickness, Reynolds stresses are assumed to be "frozen" at their upstream undisturbed values. Thus, the disturbances in this layer are inviscid in character, and to the lowest order the velocity disturbance is irrotational. However, the total flow is rotational due to the vorticity in the defect layer. Since the disturbance in this layer does not satisfy the no-slip condition at the surface, an additional inner viscous layer is required. In the inner region, which is a continuation of the upstream wall layer, the viscous and turbulent stresses are in equilibrium with the changing wall shear stress. The thickness of this layer is $O(\delta^+)$. At the interface between the wall layer and the main deck, where turbulent stress dominates viscous stress, there will be a mismatch in the turbulent stress, because on the wall layer side, turbulent stress is in equilibrium with a variable wall shear stress; on the main-deck side, it is frozen at its upstream value. Hence, a third layer, intermediate between the main deck and the wall layer, is required to resolve the mismatch in turbulent stress. This layer is called the blending layer, and here inertia terms, pressure gradient, and turbulent stress terms are of the same order. The thickness of the blending layer is $O(\epsilon^{5/2})$.

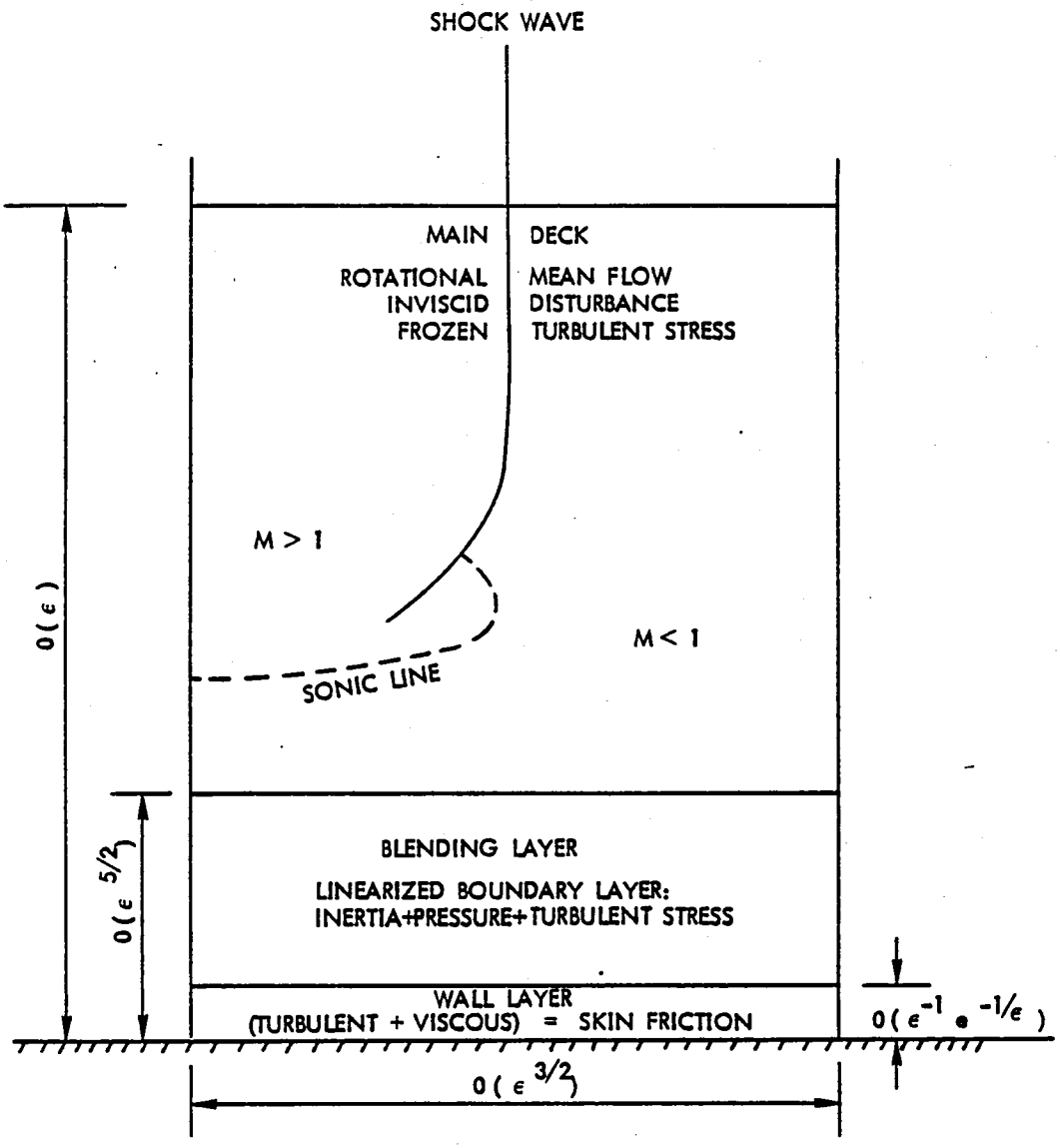

Figure 4. Schematic of the Interaction Region

Main deck - The solution in the main deck is represented by the expansion,

$$u = 1 + \epsilon[u_o(\bar{y}) + \bar{u}\ (\bar{x},\bar{y})] \tag{9}$$

$$v = (\gamma + 1)^{1/2}\ M_e\ \epsilon^{3/2}\ \bar{v}(\bar{x},\bar{y}) \tag{10}$$

where the stretched variables $\bar{x}$ and $\bar{y}$ are defined by

$$\bar{x} = x/[(\gamma + 1)^{1/2}\ M_e \epsilon\ \delta] \tag{11}$$

$$\bar{y} = y/\delta \tag{12}$$

where $x = 0$ at the shock location in the absence of interaction, and γ is the ratio of specific heats. In Eq. (9), $(1 + \epsilon U_o)$ represents the incoming boundary layer and $\epsilon\,\bar{u}$ is the perturbation produced by the shock. A disturbance velocity potential, $\bar{\phi}$, is introduced, where

$$\bar{u} = \frac{\partial \bar{\phi}}{\partial \bar{x}} \tag{13}$$

$$\bar{v} = \frac{\partial \bar{\phi}}{\partial \bar{y}} \tag{14}$$

Substitution of the above expansions into the full Navier-Stokes equations produces the following nonlinear partial differential equation for the disturbance potential:

$$[K + u_o(\bar{y}) + \frac{\partial \bar{\phi}}{\partial x}]\ \frac{\partial^2 \bar{\phi}}{\partial x^{-2}} - \frac{\partial^2 \bar{\phi}}{\partial y^{-2}} = 0 \tag{15}$$

where

$$K = \frac{M_e^{\,2} - 1}{(\gamma+1)\epsilon M_e^{\,2}} \tag{16}$$

Boundary conditions for Eq. (15) are provided by matching to the solutions in the adjacent regions. For large $\bar{y}$, the solution to Eq. (15) must approach the discontinuous normal shock solution, hence

$$\bar{u} \equiv \frac{\partial \bar{\phi}}{\partial \bar{x}} = \begin{cases} 0 & \bar{x} > o \quad \bar{y} \longrightarrow \infty \\ -2K & \bar{x} > o, \quad \bar{y} \longrightarrow \infty \end{cases} \tag{17}$$

Far upstream and far downstream, the disturbance produced by the interaction must vanish, hence

$$\bar{u} \equiv \frac{\partial \bar{\phi}}{\partial \bar{x}} \begin{cases} 0 & \text{as } \bar{x} \longrightarrow \infty, \text{ all } \bar{y} \\ -2K & \text{as } \bar{x} \longrightarrow \infty, \text{ all } \bar{y} \end{cases} \tag{18}$$

The boundary condition as $\bar{y} \longrightarrow o$ (i.e. on the surface) is provided by matching with the solution in the blending layer, details are given in (Ref. 2), and the result is

$$\bar{v} \equiv \frac{\partial \bar{\phi}}{\partial \bar{y}} = 0 \quad \text{at } \bar{y} = 0 \tag{19}$$

That means that the solution in the blending layer does not affect the v-component to order $\epsilon^{3/2}$. Equation (15) subject to boundary conditions (17), (18), and (19) is to be solved numerically for a specified value of K and a profile $u_o(\bar{y})$, e.g. law of the wake/law of the wall,

$$u_o = \begin{cases} k^{-1} \ln \bar{y} + \tilde{\pi} W(\bar{y})] & o<\bar{y}<1 \\ o & 1<\bar{y} \end{cases} \tag{20}$$

where $\tilde{\pi}$ and $W(\bar{y})$ are Coles' wake parameter and wake function.

We notice that the solution in the main deck, when expressed in terms of $\bar{x}$ and $\bar{y}$, depends only on two parameters, $\tilde{\pi}$ of the velocity profile and a similarity

parameter K. In particular the pressure coefficient has the similarity property,

$$C_p \equiv \frac{p^*(x^*,y^*) - p^*_e}{(1/2)\rho^*_e U^{*2}_e} = C_p(x,y;\ Re, Me, \gamma, U_o, \delta)$$

$$= \epsilon \bar{C}_p(\bar{x}, \bar{y};\ K, \tilde{\pi}) \tag{21}$$

where

$$\bar{C}_p(\bar{x}, \bar{y};\ K, \tilde{\pi}) = 2\frac{\partial \bar{\phi}}{\partial \bar{x}} \tag{22}$$

Thus, flows with the same values of the viscous transonic similarity parameter, K, and Cole's wake parameter, $\tilde{\pi}$, are similar.

Blending and wall layers - The flow in the blending layer is governed by linearized boundary-layer equations. The upper-edge boundary conditions are provided by matching with the solution in the main deck. It is established from the matching that the flow in the blending layer is developing under the influence of the pressure distribution given by $\bar{C}_p(\bar{x},o;\ K,\tilde{\pi})$.

In the wall layer, the governing equations reflect the fact that the total shear stress (viscous plus turbulent) is in equilibrium with the changing wall shear stress. An expression for the skin friction coefficient is obtained by matching the solutions in the wall and blending layers. The details are given by Melnik and Grossman (ref. 2), and the result is

$$C_f/C_{f_o} = (2-R)\left[1+(A_1 + A_2\,\epsilon \ln \epsilon)\,\epsilon \bar{C}_p + O(\epsilon^2)\right] \tag{23}$$

where

$$R^{-1} = \{1 + \frac{1}{2}\,\epsilon\gamma M_e^2\,[\epsilon \bar{C}_p + O(\epsilon^2)]\}$$

$$A_1 = 1/q$$

$$A_2 = 3\,[1 + (1 + m_e)q]/q^2$$

$$q = m_e^{-1/2} \quad \text{Sin}^{-1}\left[\frac{m_e}{1 + m_e}\right]^{1/2}$$

$$m_e = (1/2)\,(\gamma - 1)\,M_e^2$$

Equation (23) indicates that the shear stress variation in the interaction region is $0(\epsilon)$, so that separation of the boundary layer does not occur in the weak shock limit.

COMPARISON WITH CAHILL-CONNOR'S PARAMETERS

The analysis of the main deck shows that the important parameters that characterize the interaction are K and $\tilde{\pi}$. Recall that $\tilde{\pi}$ is a measure of the incoming velocity profile ($\tilde{\pi}$ = 1/2 for a constant pressure turbulent boundary layer), and K is a measure of the shock strength; we conclude that a successful correlation of data pertaining to normal shock boundary-layer interaction in transonic flow should include the similarity parameter K and a shape factor of the incoming velocity profile.

In the work of Cahill and Connor, experimental data of shock-induced trailing-edge separation were correlated by using a parameter, B1/2, defined by

$$B1/2 = \frac{p_\infty^*}{p_s^*}\sqrt{M_\infty - A}\ \Big/\sqrt{1 - X_s^*/C^*} \qquad (24)$$

where p_∞^* and M_∞ are the free-stream values of pressure and Mach number, p_s^* is the surface pressure immediately forward of shock, x_s^* is distance from the leading edge to the shock location, C^* is the airfoil chord, and A is a curve-fit constant.

Figure 5a. demonstrates that the variation of B1/2 with the basic parameters M_e and Re is consistent with that of K. For specific values of M_e and Re, chosen from the experimental data used by Cahill and Connor, the corresponding values of K and B1/2 were calculated and plotted in Figure 5b. It is clear from this figure that there is a correlation between K and B1/2. However, the shape of the incoming turbulent boundary layer was not accounted for in the Cahill-Connor correlation.

Part 2 of this report will study the relationship between the experimental data and the boundary layer parameters identified in this study.

$$K = \frac{M_e^2 - 1}{(\gamma+1)\,\epsilon M_e^2}$$

WHERE $\epsilon = \left(\frac{1}{2} C_{f_o}\right)^{1/2} \simeq \left(\frac{1}{L n Re}\right)$

$$B1/2 = \frac{(P_\infty / P_s)\ \sqrt{M_\infty} - A}{\sqrt{1 - (x_s/c)}}$$

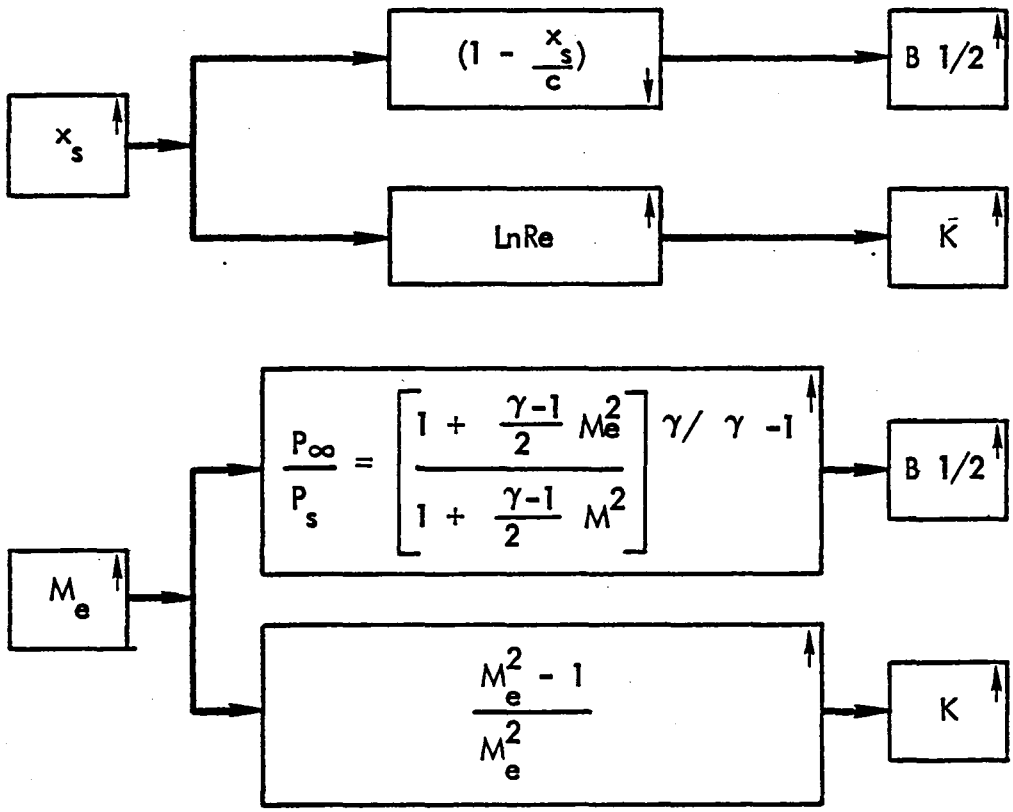

Figure 5a. Comparison of Correlation Parameters

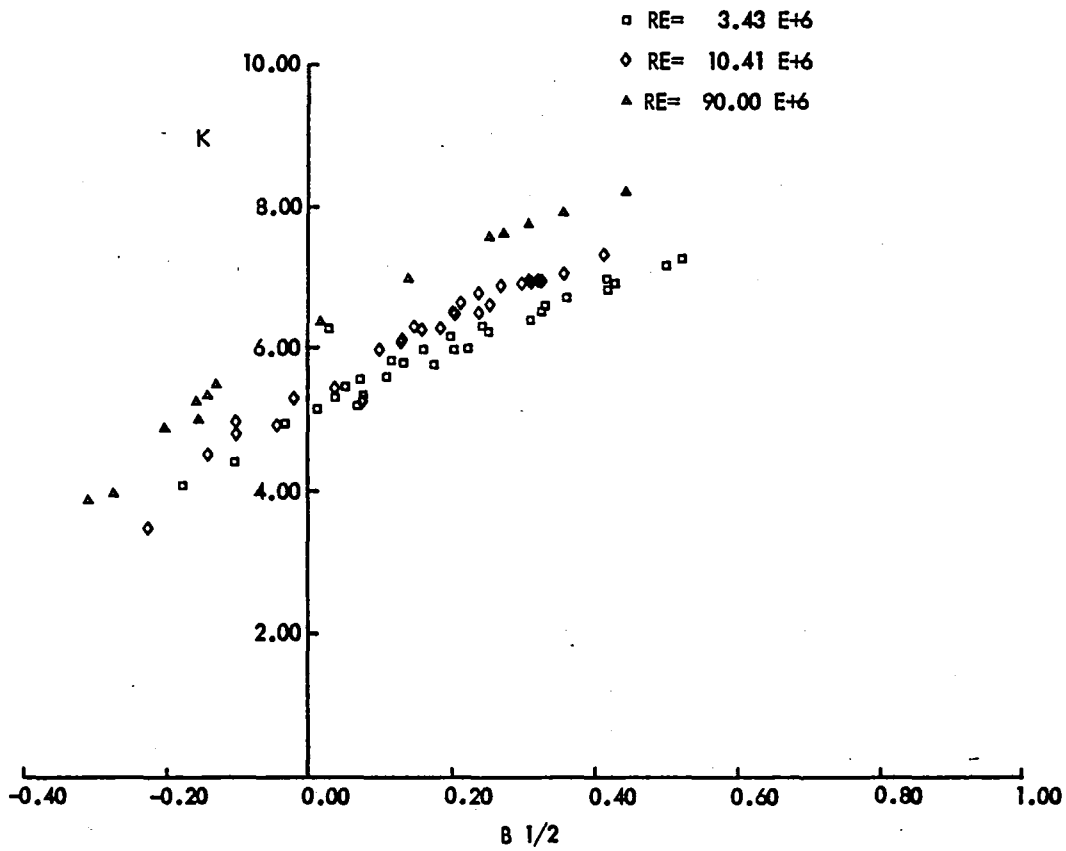

Figure 5b. Comparison of Correlation Parameters

REFERENCES

1. Cahill, J. F.; and Connor, P. C.: Correlation of Data Related to Shock-Induced Trailing-Edge Separation and Extrapolation to Flight Reynolds Number. NASA CR-3178, Sept. 1979.

2. Melnik, R. E., and Grossman, B: Analysis of the Interaction of a Weak Normal Shock Wave with a Turbulent Boundary Layer. AIAA Fluid and Plasma Dynamics Conference, Paper No. 74-598, June 1974.

3. Melnik, R. E.: Turbulent Interactions on Airfoils at Transonic Speeds-Recent Developments. AGARD-CP-291, Paper No. 10, Feb. 1981.

4. Adamson, T. C., Jr., Liou, M. S., and Messiter, A. F.: Interaction Between a Normal Shock Wave and a Turbulent Boundary Layer at High Transonic Speeds. NASA CR-3194, 1980.

PART II. REFINED EXTRAPOLATION OF WING LOAD DISTRIBUTIONS WITH TRANSONIC SHOCK-INDUCED TRAILING-EDGE SEPARATION

Jones F. Cahill

SUMMARY

An investigation has been conducted to seek improvements in a quantitative prediction of full scale transonic wing shock-induced separation data from wind tunnel test results. Previous studies had shown that such predictions can be made through use of an empirical correlation which collapses the variation of trailing-edge pressure recovery against Mach number and angle of attack into a single curve. More recently, a purely analytical correlation parameter was recommended by Mohammad Khan, based on analyses by Melnik and Grossman. In this study, that analytical correlation parameter has been used to improve the previous correlation and extrapolation process.

As a result of using the analytical parameter it was demonstrated that data influenced by local bubble separations at the shock could be isolated from those controlled by trailing-edge separations. Collapsing of the trailing-edge separation data was then shown to be much improved over previous empirical correlations. Very good correlation was shown for a series of wings varying from pre-supercritical transport aircraft types to those incorporating a full utilization of supercritical concepts.

For those cases where data are available over a wide range of Reynolds number (two "conventional" transport wings and one "moderately supercritical" wing), the scale effect on the correlated data follows a single curve. By using this newly developed information, the extrapolation of wing load data to flight Reynolds number can be accomplished with a high degree of confidence for cases which extend well into separated flow conditions.

NOMENCLATURE

A	Arbitrary constant
B 1/2	Empirical correlating parameter
C_f	Local skin friction coefficient just forward of shock
CPFOOT	Pressure coefficient at foot of shock
CPTE	Pressure coefficient at trailing edge
CPTEO	Reference value of trailing-edge pressure coeefficient
ΔCPTEO	Increment of trailing-edge pressure coefficient from its value at $R_c = 10 \times 10^6$.
H	Boundary layer shape factor
K	Analytical correlating parameter
KO	Reference value of analytical correlating parameter
ΔKO	Increment of analytical correlating parameter from its value at $R_c = 10 \times 10^6$
M	Freestream Mach number
M_e	Local Mach number at edge of boundary layer
P	Local static pressure immediately forward of shock
P_o	Freestream static pressure
R_c	Reynolds number based on local wing chord
R_θ	Reynolds number based on boundary layer momentum thickness
XCSH	Shock location, fraction of wing chord
γ	Ratio of specific heats of air
ϵ	Small perturbation parameter

INTRODUCTION

The question of scale effects on shock-induced trailing-edge separations has been a serious concern since the 1960's when comparisons between wind tunnel and flight test data first indicated serious discrepancies. In 1968, Pearcey, Haines, and Osborne published Reference 1, in which the distinction was made between modern (at that time) heavily loaded wings that experienced those discrepancies resulting from separations originating at the trailing edge, as opposed to earlier, more conservatively designed wings, that separated only as a result of the expansion of bubble separations originating at the shock. Those earlier wing types had previously been shown to be free of scale effects if wind tunnel tests were made at Reynolds numbers of at least 1.5 million and if turbulent boundary layers at the shock were assured. With separations originating at the trailing edge, shock location differences of 20% chord or more have been observed between wind tunnel and flight conditions. The resulting changes in lift and pitching moment cause large changes in airloads on the wing structure, and large changes in tail load required for trim.

A considerable effort has been devoted to this subject since that time. In 1971, an AGARD conference (Reference 2) was devoted to test facilities and techniques for high Reynolds number investigations at transonic speeds in recognition of this and other transonic scaling problems. High Reynolds number wind tunnels are now being constructed both in this country and in Europe.

In spite of the forthcoming availability of wind tunnel facilities for investigations of this subject, there is still a need for analytical and empirical methods to evaluate scale effects on these aerodynamic phenomena. Much testing will continue to be accomplished in low Reynolds number facilities and it must be possible to predict aerodynamic data for flight conditions from results of those tests even if later tests will be performed in the newer facilities. Furthermore, some of the new facilities will not match flight Reynolds numbers for large aircraft and extrapolation will still be required.

A method for prediction of the scale effects in this area was evolved at Lockheed, and in 1979, Reference 3 was published with an extended version of that method. This prediction was based on an empirically derived correlation of the development of trailing-edge separation which for each spanwise station on a wing, collapses the variation of trailing-edge pressure recovery with Mach number and angle of attack into a single curve. The variation with Reynolds number of this curve has been found to be rather straight-forward and to be identical for a wide variety of wing designs.

More recent effort on this subject has resulted in a recommendation by Mohammad Khan (Reference 4) that the similarity parameter K, which had previously been discussed by Melnik and Grossman, should be an appropriate correlation parameter for this phenomenon. It is the purpose of this report to discuss evaluations of that correlation parameter against a large bank of previously available experimental data, and to provide further refinements of the entire correlation and extrapolation method.

REVIEW OF PRIOR CORRELATION CONCEPT

The scale effect extrapolation method presented in Reference 3 depended on several empirical correlations and generalizations which were sufficienty convincing that the extrapolation process could be approached with confidence. Current effort on this subject is intended to increase that confidence by attempting to put the correlation on a firmer scientific foundation (see Reference 4), and to refine and expand the technique. Since the basic extrapolation concept is not changed in this process, the following paragraphs will review those correlations and generalizations.

The outstanding discrepancies observed between wind tunnel and flight data in this area have been large increases in local lift and pitching moment on the wing for conditions which experience separations in the wind tunnel but are unseparated at flight Reynolds numbers. By observing pressure distribution measurements, it quickly became apparent that when the wing trailing edge separated, the shock moved forward. Local separations at the shock might be followed by reattachment, but no perturbation of shock location was noted unless the trailing edge separated. Trailing-edge pressure coefficient has therefore been used throughout as an indicator of significant separations.

Variation of Shock Location with Trailing-Edge Pressure Coefficient

The relationship between trailing-edge pressure coefficient and shock location has been found to be adequately defined by a single curve for a given Mach number at a given location on a particular wing. Figure 1 shows such curves defined for a single case at two different Mach numbers. In each case, data from a bare wind tunnel model, from that model with vortex generators on the wing upper surface at 55% chord, and from flight tests are shown. Within an acceptable scatter, these data form a single curve for each Mach number, establishing a unique relationship so that when trailing-edge pressure is known, shock location can be estimated to a reasonable accuracy. In this case, changes in angle of attack did not result in significant deviation from the single curve. In the data examined to date in fact, no case has shown significant deviations. Intuitively, it would seem that cases might exist for

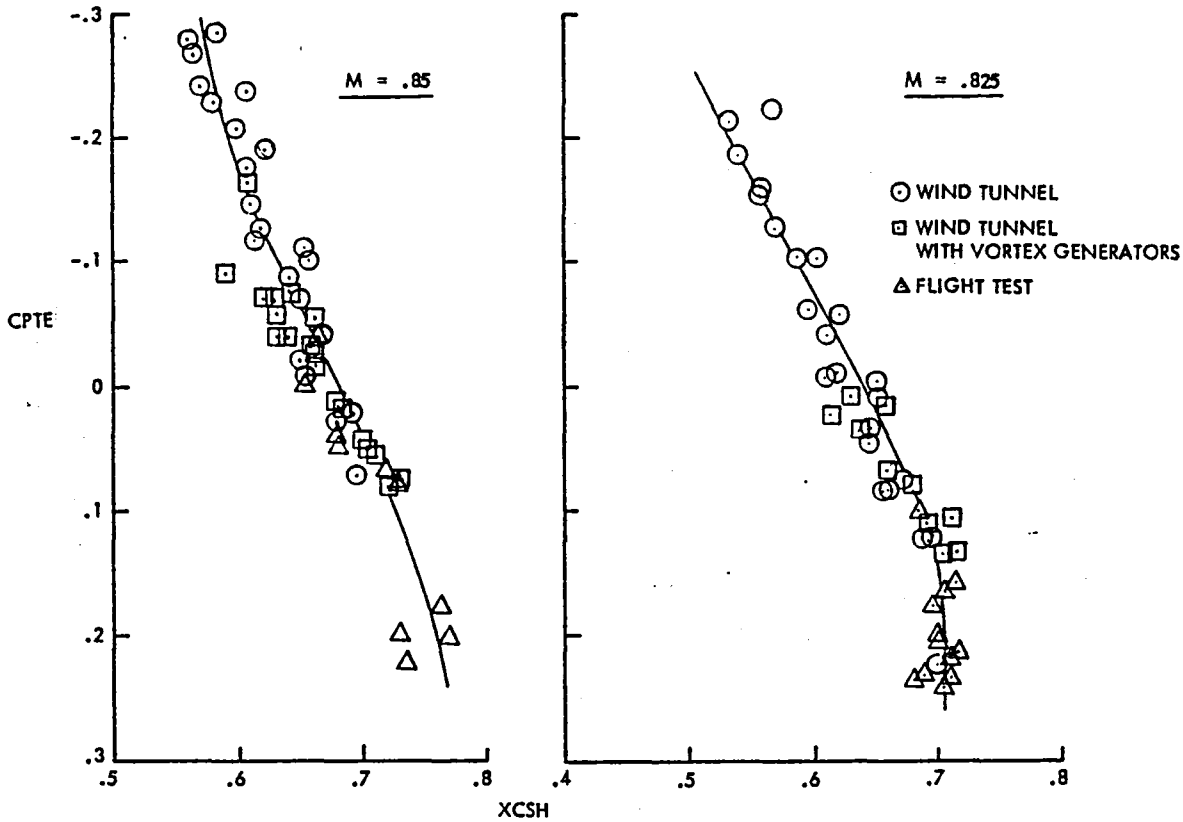

Figure 1. Variation of Shock Location with Trailing Edge Pressure Recovery

which angle of attack might need to be accounted for as an additional variable. Such variations could be accommodated in application of this method with only a slight increase in effort.

EMPIRICAL CORRELATION

As stated previously, the correlations of shock-induced separation data described in Reference 3 were purely empirical, they were evolved simply from a recognition that the pressure rise through the shock and through the subsequent subsonic pressure recovery must be the outstanding factors in determining the occurrence and severity of any resulting separation. Additional terms were added to the correlation parameter and the form of the parameter presented in Reference 3 was the result of several iterations. It was successful in collapsing (to a convincing degree), data from C-141 and C-5 wind tunnel and flight data, wind tunnel data on a "moderately supercritical" wing developed by the RAE in the United Kingdom, and flight data on the F-8 airplane which had been modified by NASA to explore the characteristics of supercritical wings. That correlation parameter,

$$B1/2 = \frac{Po/P\ \sqrt{M\ \ -A}}{\sqrt{1-XCSH}}$$

contained the arbitrary constant A which was used to accomplish the final tailoring of the correlations. A value of A was selected to minimize the scatter in the data being correlated. All of the available data were included in the correlations, and although it was known that those data included cases involving a variety of modes of separation, no attempt was made to discriminate among those modes. While it was apparent from the density of points clustered around the correlation curves that the separation development was being collapsed into a single curve which could then be further utilized to account for scale effects, the number of test points which eluded collapsing was disappointing. Furthermore, in some cases (see Figures 20 and 23 in Reference 3 for the RAE wing model at Wing Station η = 0.793), the departure from the correlation curve was obviously a systematic effect influencing only

a specific group of test conditions. These partial failures of the empirical correlation parameter, coupled with the fact that an analytically supported correlation would be perceived as more rigorous and therefore more universally applicable, provided a major incentive for this, and the associated study reported in Reference 4.

Scale Effect on the Correlated Separation Development

The real key to successful extrapolation of the wind tunnel data to flight conditions is the fact that the shape of the curve describing the development of trailing-edge separation is independent of Reynolds number. This fact is illustrated in Figure 2 where data for one station of the C-141 wing are shown for a number of Reynolds numbers from both wind tunnel and flight tests. As the Reynolds number is increased, the curve moves bodily to more positive values of CPTE and P. In this subsection P refers simply to a given correlating parameter, PO to a reference value of that parameter, and Δ PO to the variation of PO from its value at a Reynolds number of 10×10^6. The comments herein apply equally to the empirical parameter B 1/2 and the new analytical parameter K. Figure 3 (top left) shows this shift by superimposing the curves into a single plot.

The scale effect can now be fully described by plotting values of CPTEO and PO, at the break in the separation development curve, against Reynolds number. As shown in Reference 3, these variations were sufficiently similar for a wide variety of wings that a single curve could be used for all of the data available. These scale effect plots are reproduced at the bottom of Figure 3 as increments of CPTEO or PO from their values at $R_c = 10 \times 10^6$.

A graphic demonstration of the validity of these concepts can be obtained by subtracting the appropriate values of CPTEO and PO from all of the data for each Reynolds number. By this means, the data are all collapsed into a single curve which provides a substantial validation of the curve shape and its independence of Reynolds number. A sample of such plots is shown at the top right of Figure 3.

The analysis presented in Reference 3, therefore, demonstrated the feasibility of collapsing the variation of trailing edge pressure recovery with angle of attack and Mach number into a single curve. It was shown further

that the effect of changing Reynolds number on that correlated data could be described rather simply and the scale effect on shock-induced trailing edge separation could, therefore, be reasonably extrapolated.

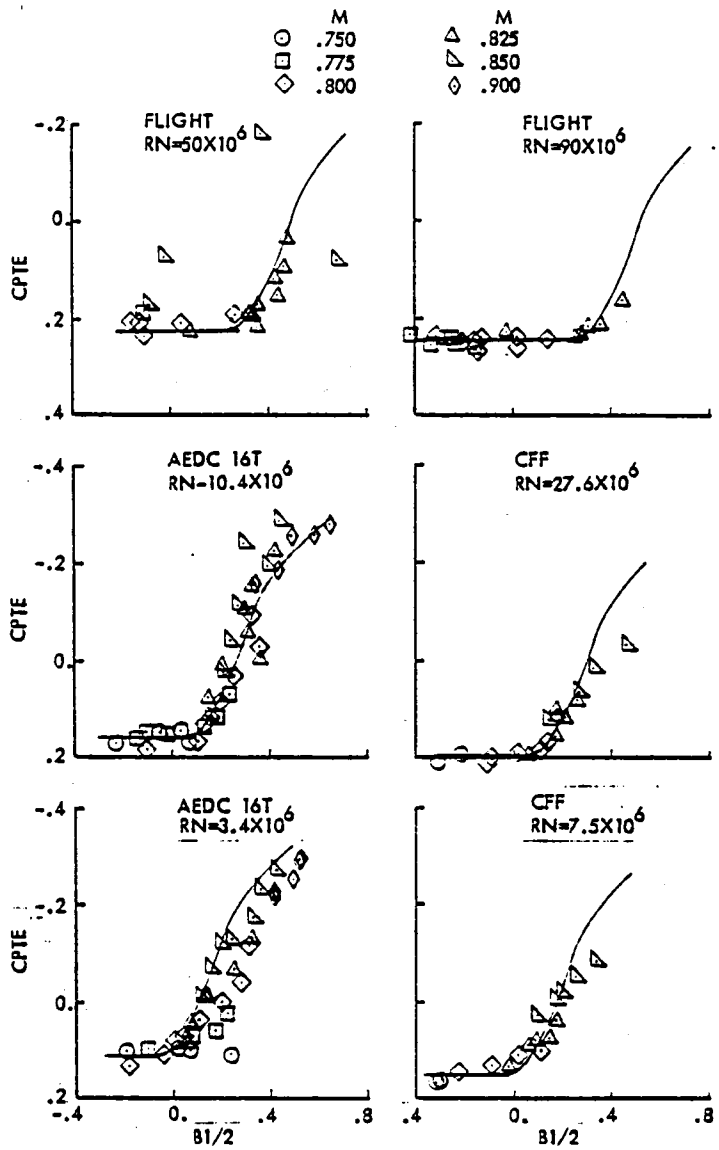

Figure 2. Basic Correlation C-141, η = .193, A = 1.50

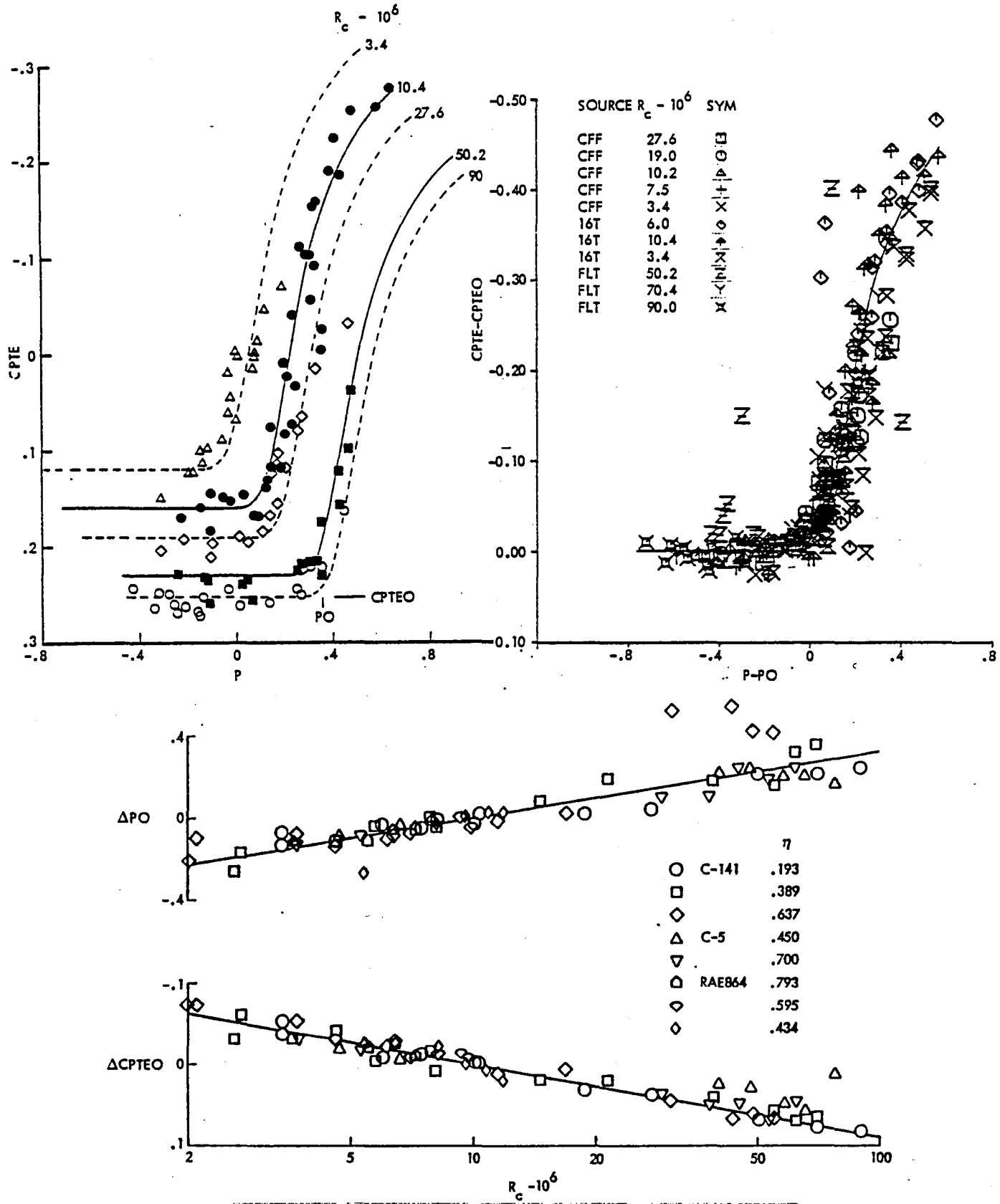

Figure 3. Reynolds Number Variation of Correlated Data

EVALUATION OF ANALYTICAL CORRELATION PARAMETER

The correlation parameter derived in Reference 4 is defined as:

$$K = \frac{(M_e^2 - 1)}{(\gamma + 1)\epsilon M_e^2} \qquad \text{Where: } \epsilon = \sqrt{C_f/2}$$

and M_e and C_f are, respectively, the boundary layer edge Mach number and skin friction coefficient immediately ahead of the shock. The Mach number, M_e, is defined for the flow direction normal to the local element (constant percent chord) line of the wing as an approximation to the flow direction normal to the shock. Since this parameter provides some accounting for the condition of the boundary layer through the inclusion of the term C_f, the possibility exists that it could produce significantly improved correlations. Skin friction coefficients for the correlation parameter were calculated using the method presented in Reference 5.

Initial attempts to assess the correlation of separation development using the parameter, K, met with mixed results. Data for Station η = 0.193 of the C-141 wing, which are shown in Figure 4, indicate an excellent collapsing of data in the case of both the empirical parameter B1/2 and the analytical parameter K. Data in Figure 5 for Station η = 0.434 of the RAE 864 wing, on the other hand, had produced rather a poor correlation with the empirical parameter, and the analytical parameter now groups the data into two distinct and rather well defined variations. Data are shown in Figure 4 for only a single Reynolds number. Similar comparisons made at other Reynolds numbers produce the same conclusion. Figure 5 contains data from all of the Reynolds numbers for which these tests had been conducted. Data in the abrupt decrease in pressure recovery for values of K near 4.5 are all from tests at a local chord Reynolds number of 5.5×10^6. All of the remaining data collapse into a reasonably tight band showing the deterioration in pressure recovery at significantly higher values of K. The reasons for this different behavior were sought in a detailed examination of the basic data from which these correlations had been developed.

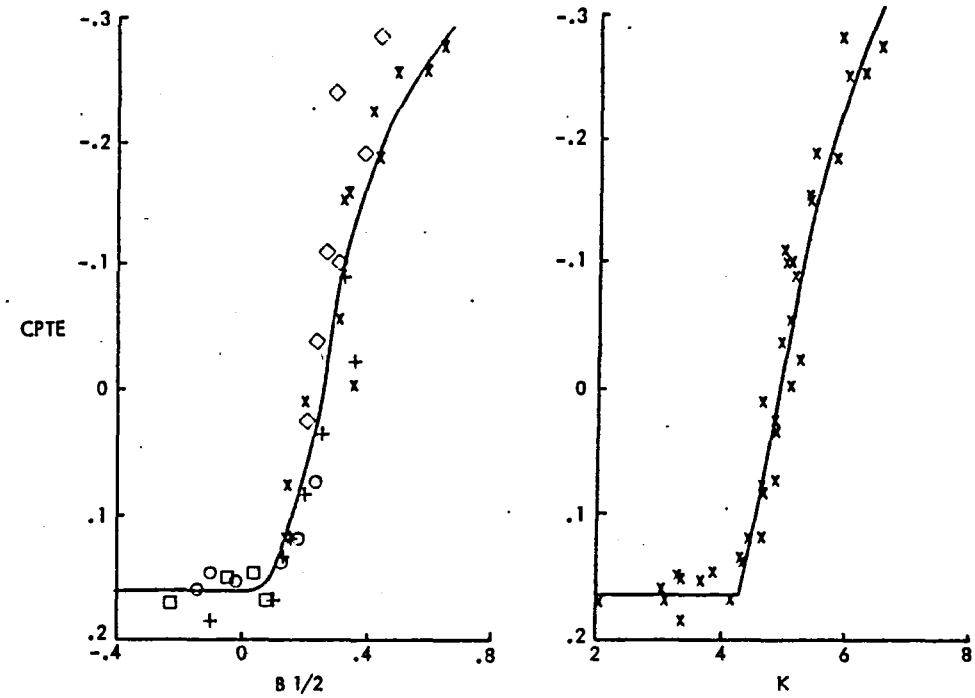

Figure 4. Comparison of Correlations. C-141 Wing, η = .193, R_c = 10.4 X 10^6

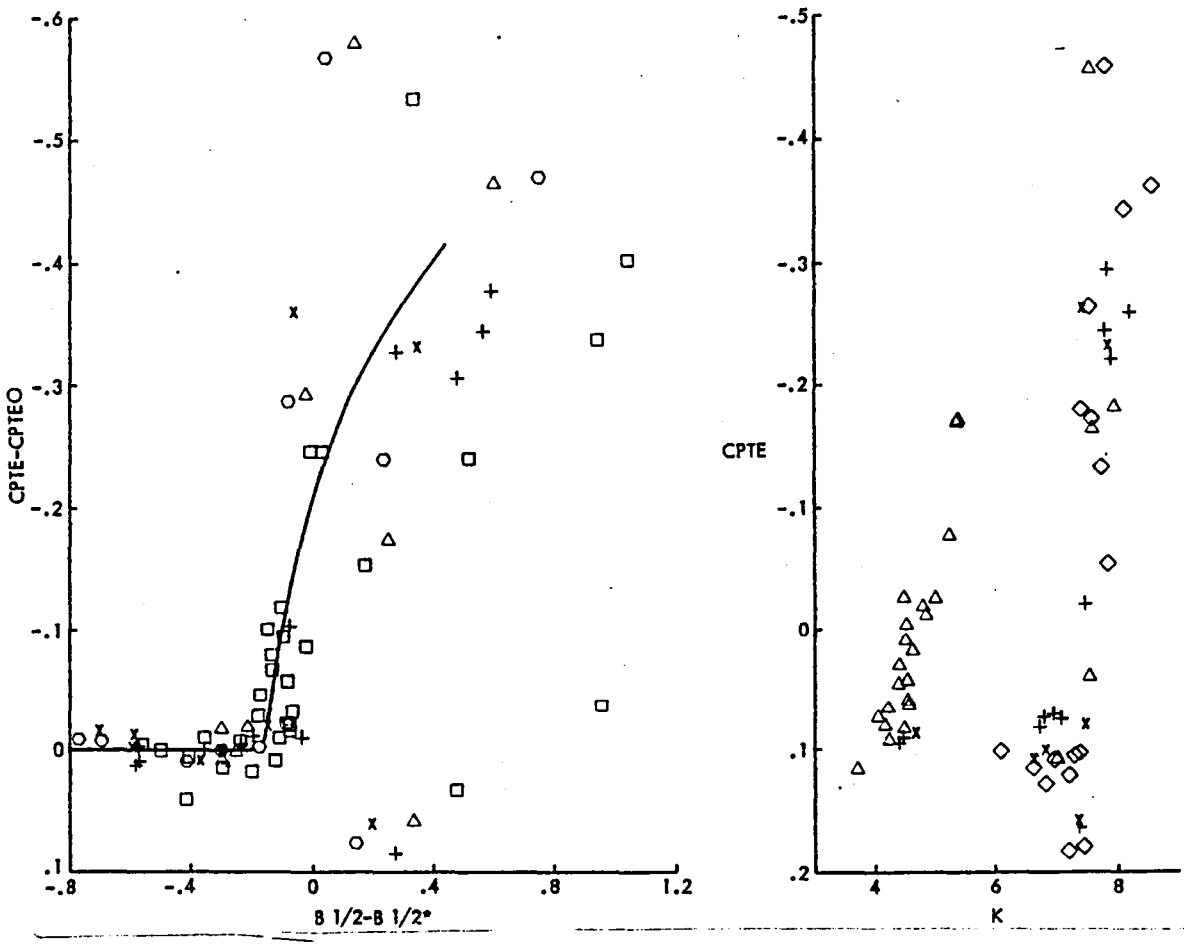

Figure 5. Comparison of Correlations. RAE 864 Wing η = .434, R_c = 5.5 TO 12 X 10^6

Local Separation at the Shock

The progression of separation development with variations in angle of attack is shown for several Mach numbers in Figure 6 using data for a single Reynolds number from Figure 5. As the angle of attack is increased, the trailing-edge recovery deteriorates along a curve very much like the usual correlations illustrated by Figure 4. At an angle of attack near 4°, the curve is suddenly displaced to a significantly higher value of K at the same, or a somewhat improved pressure recovery. Further increase in angle of attack shows the pressure recovery deteriorating further along a new curve.

Figure 7 shows plots of the chordwise pressure distribution for the Mach number 0.85 points of Figure 6. The displacement to the higher values of K between angles of attack of 3° and 4° is obviously associated with the appearance of a separation bubble at the shock which is indicated by the local supersonic Mach number at the shock foot and the concave shape of the pressure distribution downstream of the foot. In this instance, the separaton bubble appears very suddenly as a result of the downstream sweeping of a root shock on this wing. The merging of the root shock with the shock terminating the local supercritical region of the upper surface flow causes an abrupt increase in the pressure rise through the terminal shock and therefore produces the local separation. Similar pressure distribution data for a Mach number of 0.875 are shown in Figure 8. The fact that the departure from the normal correlation is a result of the presence of the separation bubble rather than the simple merging of shocks as illustrated in Figure 9 where data are presented for Station η = 0.45 of the C-5 wing showing a more gradual bubble development in the absence of a root shock. Presence of the separation bubble causes a deviation from the basic correlation curve in this case just as it does in the other cases presented previously.

Figure 10 shows pressure distribution plots illustrating the character of the separation development on the C-141 wing at Station η = 0.193. In this case, the trailing-edge separation (indicated by a deterioration in pressure recovery) is obviously the dominant separation mode. A separation bubble is apparent at the foot of the shock, if at all, only after the trailing-edge separation has become quite pronounced. A close examination of all the data available for this case (η = 0.193), in fact, shows that separation bubbles

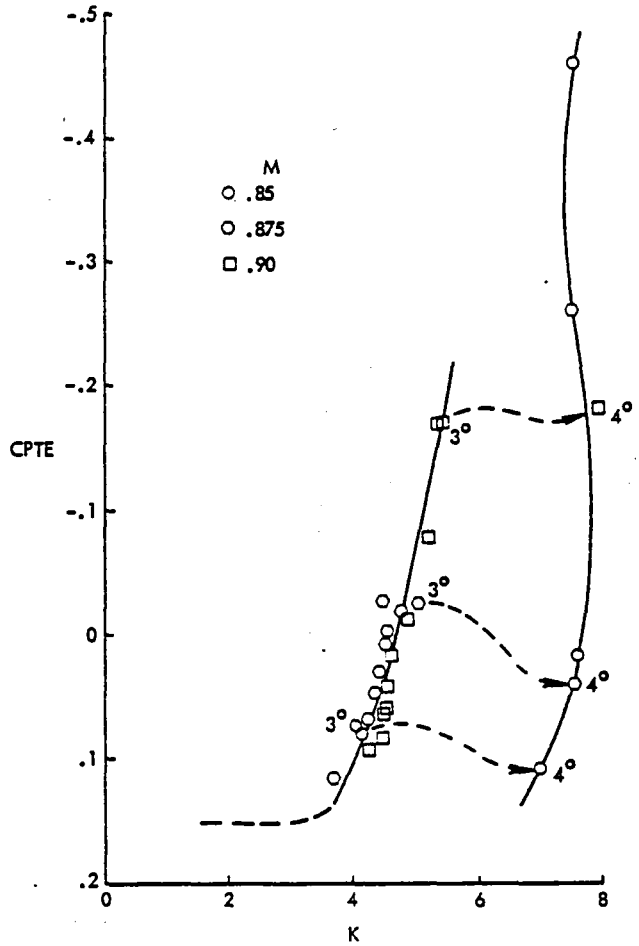

Figure 6. Details of Separation Development. RAE 864 Wing, $\eta = .434$, $R_c = 5.5 \times 10^6$

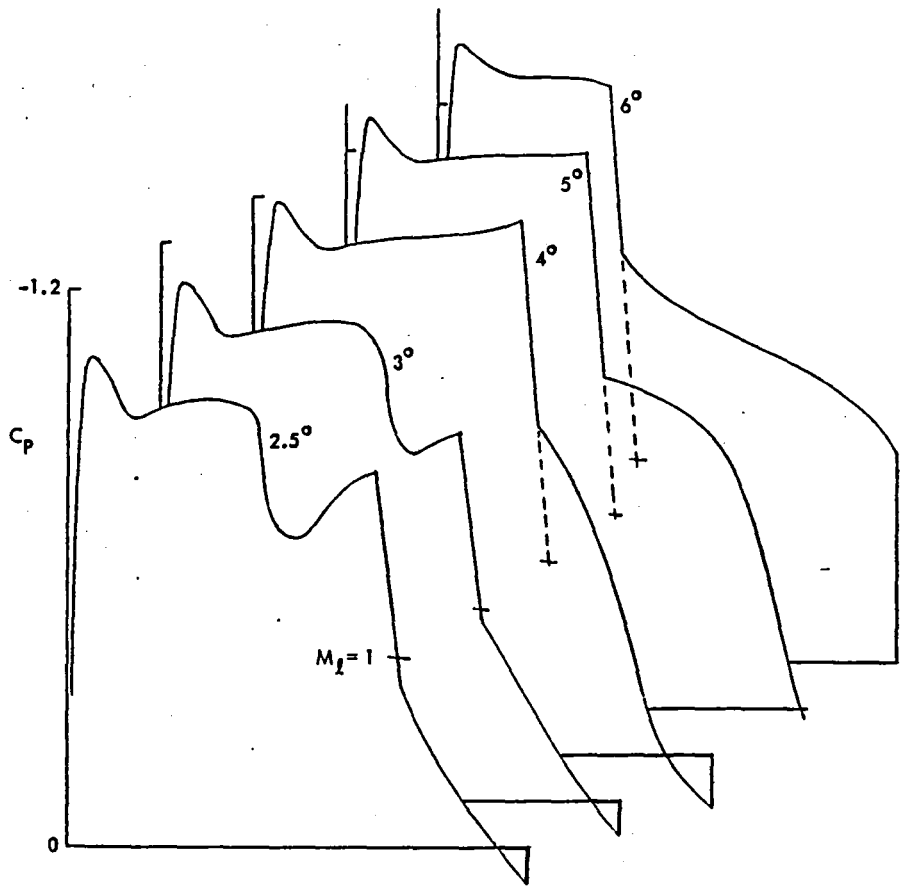

Figure 7. Illustration of Separation Bubble Development.
RAE Wing 864, $\eta = .434$, $R_c = 5.5 \times 10^6$, $M = 0.85$

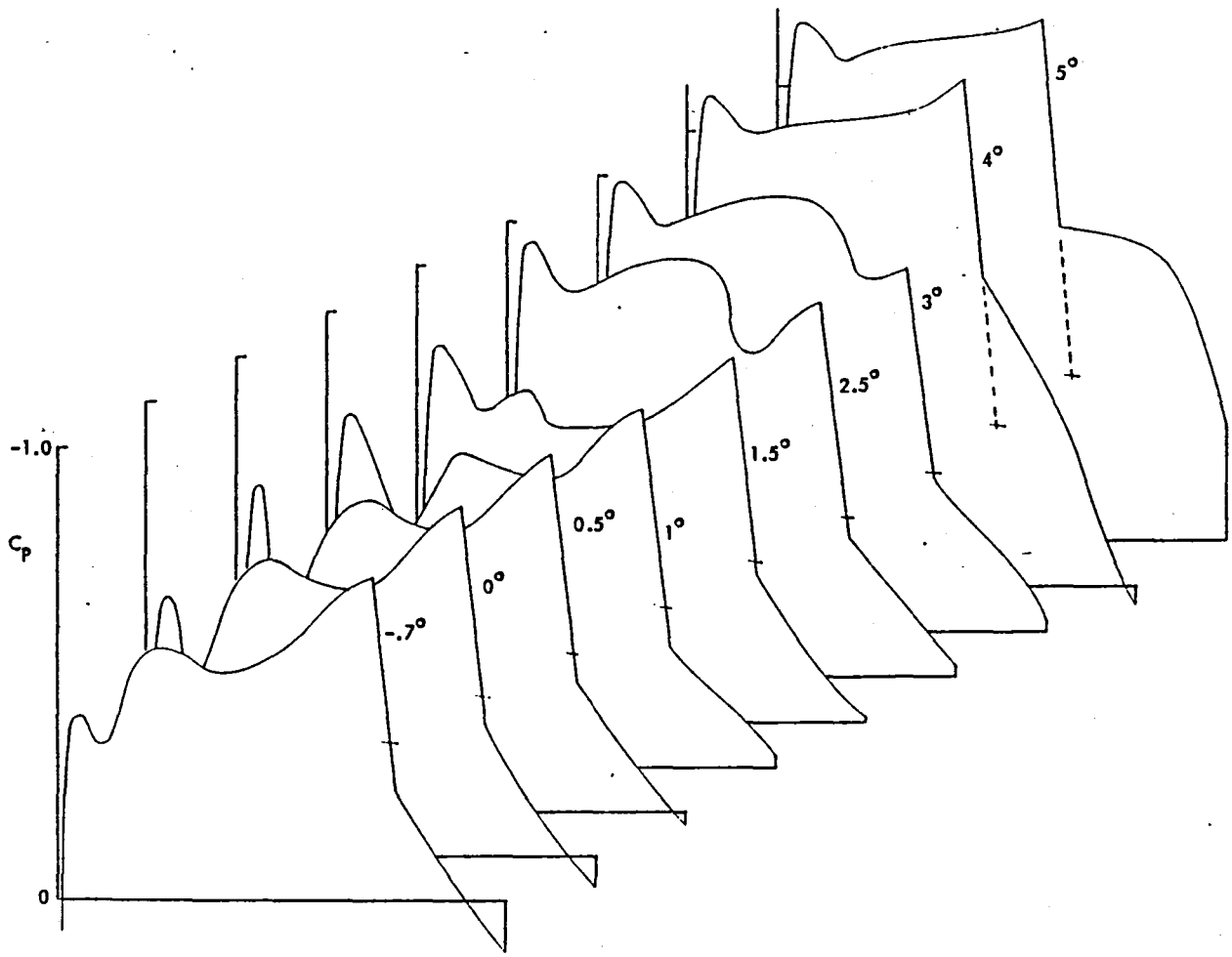

Figure 8. Illustration of Separation Bubble Development.
RAE Wing 864, $\eta = 434$, $R_c = 5.5 \times 10^6$, $M = .875$

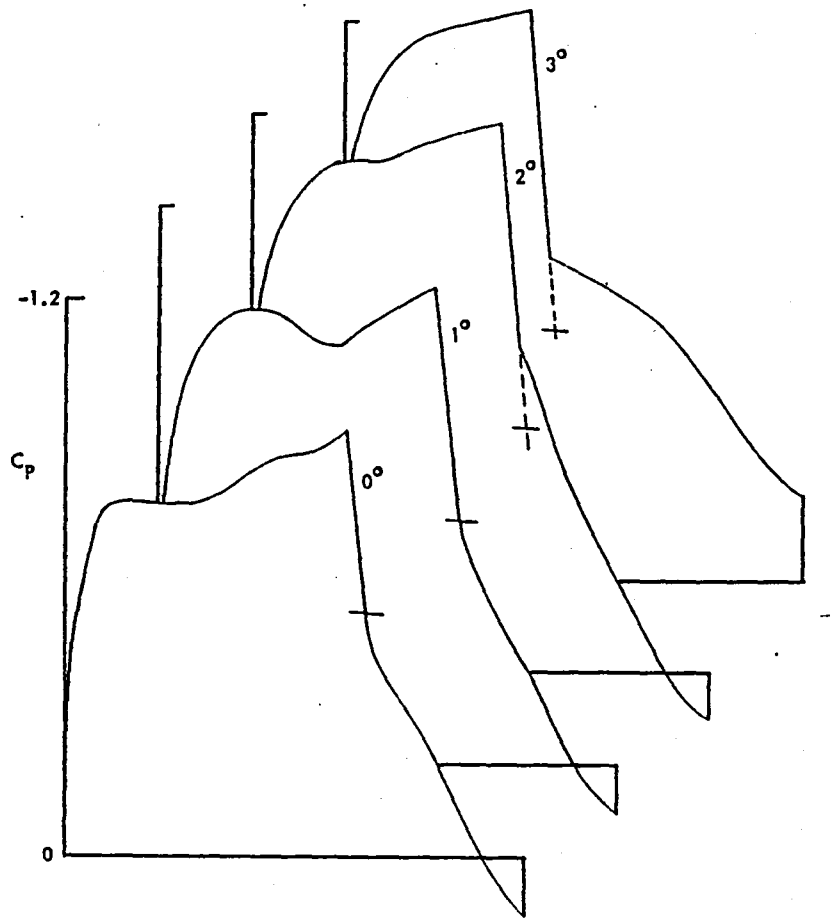

Figure 9. Separation Bubble Development in Absence of Root Shock. C-5 Wing, $\eta = .45$, $R_c = 6.6 \times 10^6$, $M = .80$

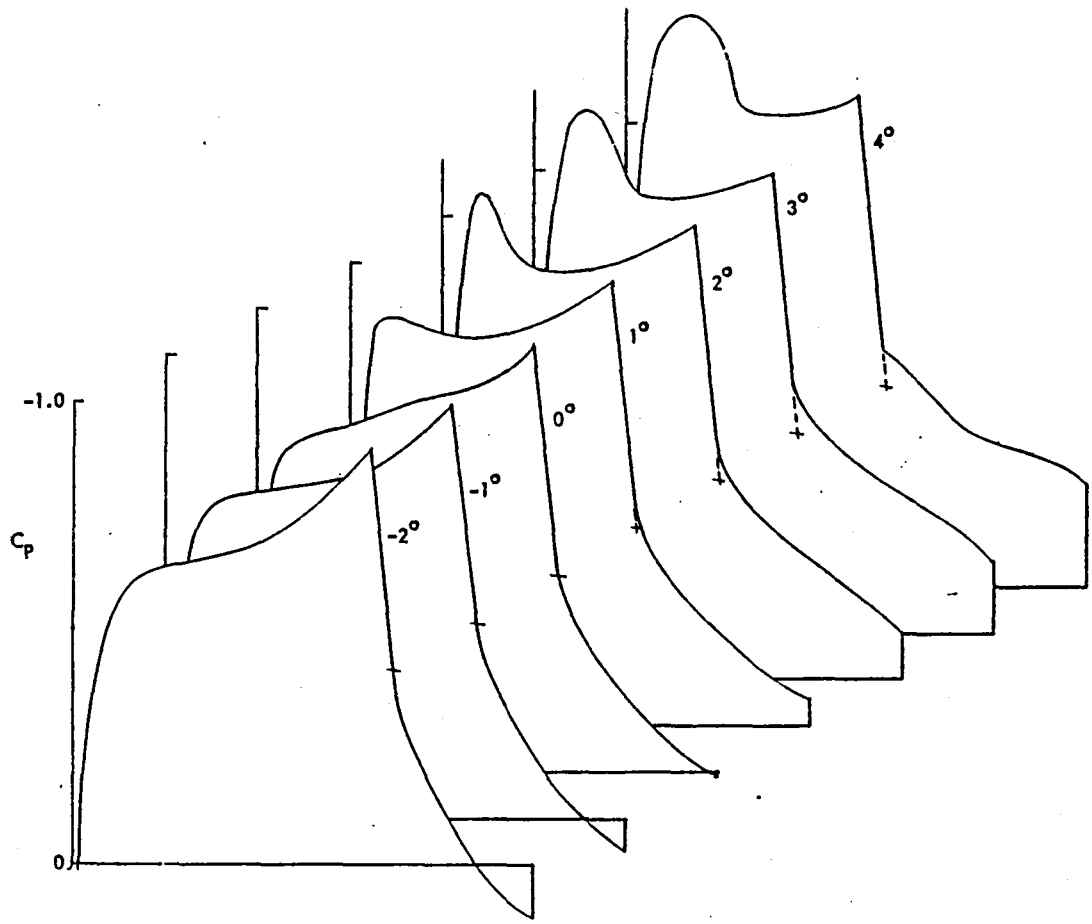

Figure 10. Trailing Edge Separation Development. C-141 Wing, $\eta = .193$, $R_c = 10.4 \times 10^6$, $M = .825$

at the foot of the shock occur very rarely and the correlations shown in Figure 4 are typical of those observed for that wing station in all of the various pressure tests made on the C-141 wing.

The pressure distributions for all of the data available for analysis in this study have been reviewed to determine those cases affected by the presence of separation bubbles at the shock foot. During this review, the connection between bubble separations, as indicated by the shape of pressure distributions, and deviation from the basic correlation plots was strongly reinforced. Another fact also became obvious however. As angle of attack or Mach number are increased beyond the initial separation, the eventual situation is a separation of the entire flow from the shock to the trailing-edge. At that point, the bubble separation conditions should return to agreement with the basic correlation curve which is related to cases where separations initiate at the trailing-edge. This is in fact the case as indicated by the data. A simple criterion was evolved to define those points to be retained as a result of observing a large number of these data points. This criterion is illustrated by the plot shown in Figure 11 where the slope

$$\frac{CPFOOT - CPTE}{1-XCSH}$$

is plotted against the value of the correlation parameter K for a number of test conditions. Above the upper curve, nearly all points deviate from the basic correlation curve. Below the lower curve, nearly all points agree. In the intermediate range between the two lines, it is impossible to discriminate. This criterion was used to determine whether to retain each of the data points for which the pressure distribution shape indicated the presence of a separation bubble. Those points falling between the two lines on Figure 11 were retained if they were in reasonable agreement with the correlation curve. It should be emphasized that this criterion is not an aerodynamic assessment of which points should be included with the bubble separation cases. It simply uses a low value of the slope of the pressure distribution downstream of the shock as an indicator of complete separation.

Exercising the obvious conclusion from the foregoing discussion, only those data points in Figure 5 which show an abrupt deterioration in pressure

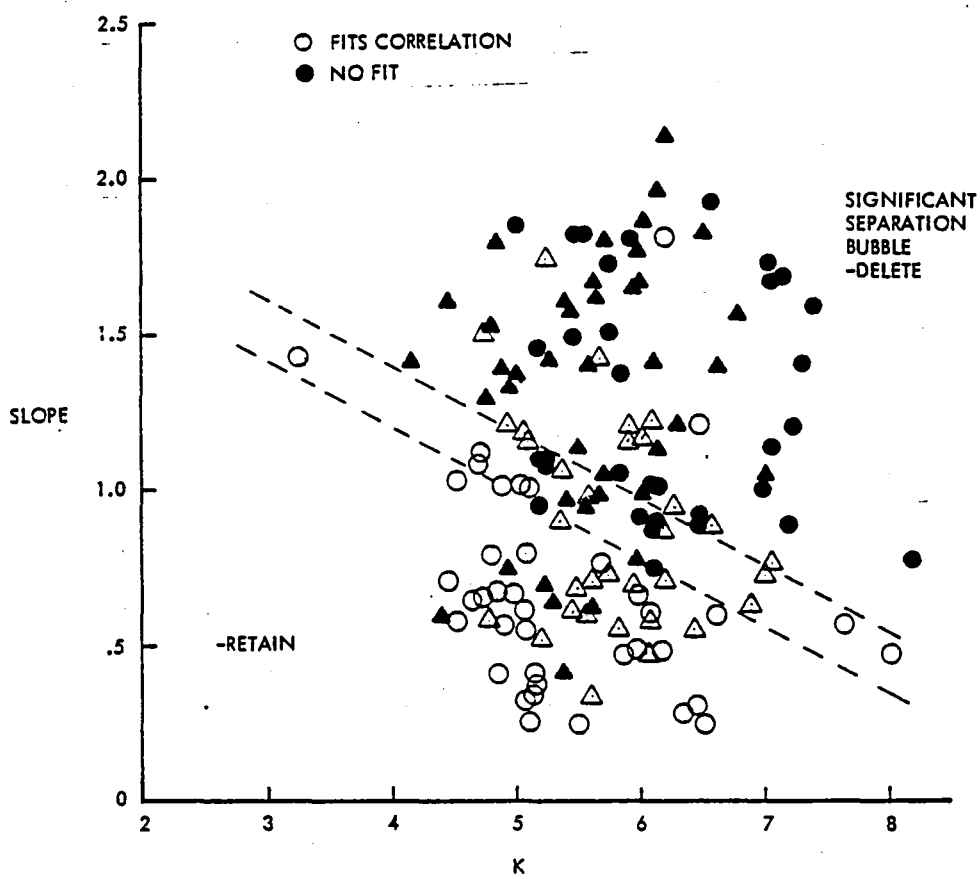

Figure 11. Criterion for Retention of Bubble Separation Cases

recovery at values of the correlation parameter K near 4 to 4.5 should be retained in this study. The remaining points are dominated by the separation at the foot of the shock and are not solely dependent on trailing-edge separations. Figure 12 shows data from several other cases. For each case shown, the plot on the left contains all measured test points, the plot on the right contains the test points remaining after deletion of those points experiencing bubble separations at the shock foot. This sampling of available data showing only those points dominated by trailing-edge separation provides a strong substantiation of validity of the analytical correlation parameter K suggested by Khan in Reference 4.

The distinctions just discussed between shock-induced separation developments which are dominated on one hand by trailing-edge separation and on the other hand by local separation bubbles near the shock should not be surprising in view of the differences pointed out by Pearcey, Haines, and Osborne in Reference 1. In that reference, the very substantial differences in behavior between Model A flows where separations initiate at the foot of the shock, and Model B flows where separations initiate at the trailing-edge are clearly displayed. The ambiguity inherent in the presence of the arbitrary constant A in the empirical parameter of Reference 3 allowed data to be artificially compressed in a number of cases so that a conclusion of complete generality seemed warranted by the reasonably tight collapsing of points displayed by the preponderance of data considered. The uniqueness of the analytical parameter K precludes this artificial compressing and leaves the unquestionable indication of two distinctly different phenomena which is provided by Figure 5.

The conclusion reached in Reference 1 was that significant scale effects should be anticipated for Model B flows, but that in the case of Model A flows, wind tunnel data obtained with turbulent boundary layers should properly represent the flight condition in spite of large differences in Reynolds number. The data points showing the deterioration of pressure recovery at high values of K in Figure 5 would tend to support that conclusion. Data measured over a range of Reynolds numbers from 5.5×10^6 to 12×10^6 fall within a rather narrow band.

In handling wind tunnel data during evaluation of a new configuration, those data points suffering significant separations at the shock are readily

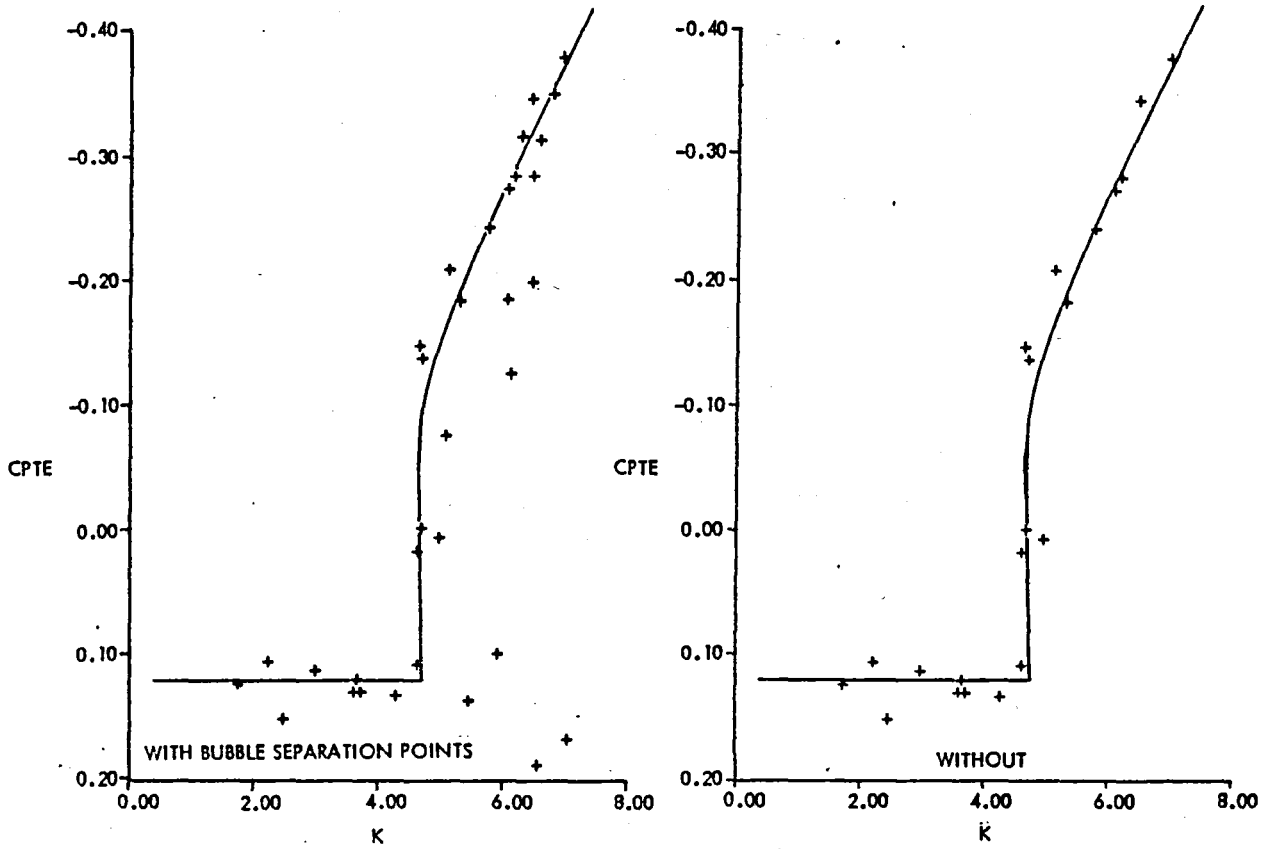

a C-5 Wing, ETA = .45, $R_c = 6.6 \times 10^6$

Figure 12. Comparison of Correlations with and without Bubble Separation Points

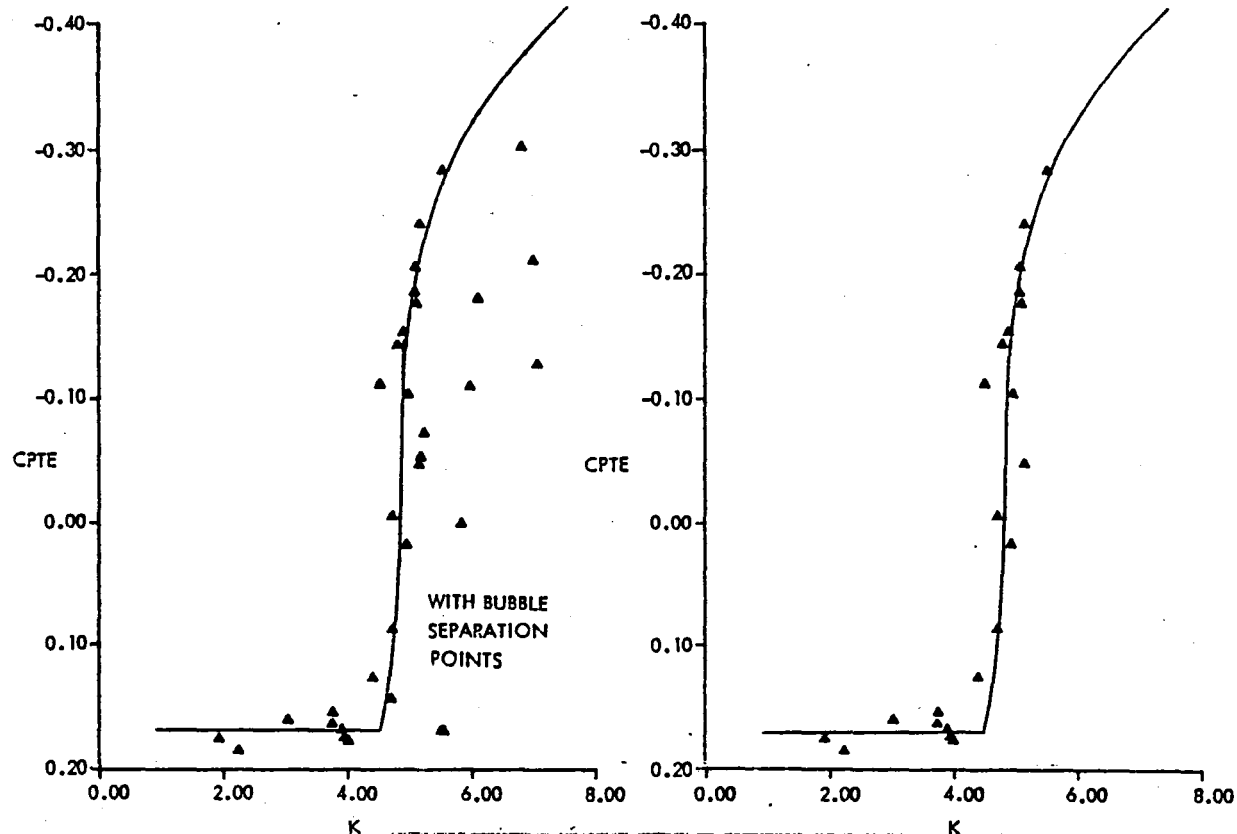

Figure 12.b C-5 Wing, ETA = .70, $R_c = 5.3 \times 10^6$

recognized by the fact that measured pressures near the foot of the shock indicate supersonic velocities. As a result of the flow around the bubble, the shape of the pressure distribution in this region tends to become convex. Figures 7, 8 and 9 are good guides to the pressure distribution changes which accompany separation bubble appearance. The pressure distribution points experiencing separation bubbles are simply set aside during the Reynolds number extrapolation process and then re-integrated with the extrapolated data.

Exceptional Pressure Recovery

In a number of instances, the separation bubble at the foot of the shock occurs prior to any trailing-edge separation. In many of these instances, the trailing-edge pressure recovery improves by a noticeable increment. Such cases are illustrated In Figure 5, where the highest normal recovery, at low values of K or B1/2, is 0.1 to 0.12. Following the onset of the bubble separation, the trailing-edge recovery increases to 0.175 or 0.185. No measurements are available to demonstrate the mechanism by which this improvement is developed. It is possible that turbulence induced by the separation and reattachment results in an entrainment by the boundary layer of higher energy flow and, therefore, in an effect comparable to that produced by vortex generators. Reference 6 discusses several mechanisms by which boundary layer turbulence is amplified in passing through a shock wave.

Low-Speed Stall

Data presented in Figure 23 of Reference 3 for wing station η = 0.793 of the RAE Model 864 wing showed an outstanding example of data points in a narrow range of test conditions for which the empirical correlation failed completely. The majority of test points for this station collapsed rather nicely in terms of the empirical parameter B1/2, but high angle of attack data for the lowest Mach number tested (0.785) consistently departed from the collapsed curve. Correlations in terms of the analytical parameter K produced the same result. Figure 13 shows a series of pressure distribution plots for test conditions which encounter this kind of departure. For angle of attack up to 3.4°, the shock is a well defined, nearly instantaneous, pressure rise

which is preceeded by a leading-edge pressure peak and a small shock-free recompression. At 3.7° angle of attack and above, the well defined recompression and shock give way to a single smoothed-out pressure recovery similar to that experienced near low-speed maximum lift conditions. The precise mechanism producing the pressure recovery from supercritical to subcritical flow in these cases is not known, but the pressure distribution shapes give the impression of a merging of many weak waves originating in the flow near the leading edge rather than a discrete shock-type pressure rise. These cases therefore experience phenomena significantly different from the more usual transonic shock cases and, therefore, fail to correlate. Pressure distributions for all available data have been surveyed, and those data points that show low-speed stall characteristics of this kind have been deleted.

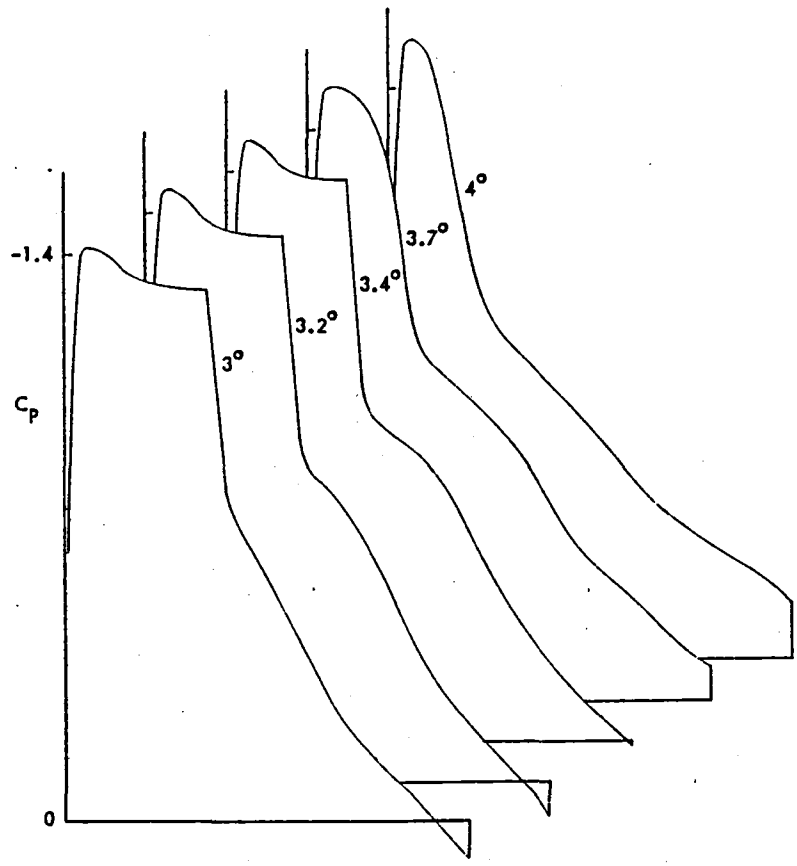

Figure 13. Illustration of Low Speed Stall Characteristics for Low Mach Numbers and High Angles of Attack. RAE Wing 864, $\eta = .793$, $R_c = 3.7 \times 10^7$, $M = .785$.

SUMMARY OF DATA CORRELATIONS

A thorough evaluation of the correlating parameter, K has been performed by correlating all of the data previously considered in Reference 3. The following data sets are included: (1) Wind tunnel and flight data for several stations of the C-141 and C-5 wings, (2) three stations on a wind tunnel semi-span wing model called the RAE Model 864, (3) data from two spanwise stations on the wing of the F-8 SCW research airplane which was developed and flown by NASA to demonstrate supercritical wing technology. The RAE Model 864 wing has been called moderately supercritical, it shows high aft loading resulting from a cusped aft lower surface and some isentropic recompression before the shock. This group of data sets, therefore, covers a wide range of wing types and as will be shown by the data which follow, the parameter K is successful in collapsing data for all of these cases.

Data points suffering either from separation bubbles at the shock or from low speed stall characteristics were deleted and composite plots were prepared with the data from all of the test Reynolds numbers collapsed into a single curve by subtracting from the data measured at any given Reynolds number, the values CPTEO and KO which are used to describe the Reynolds number effects on the correlated data. Definitions of the reference values CPTEO and KO are illustrated in the sketch below.

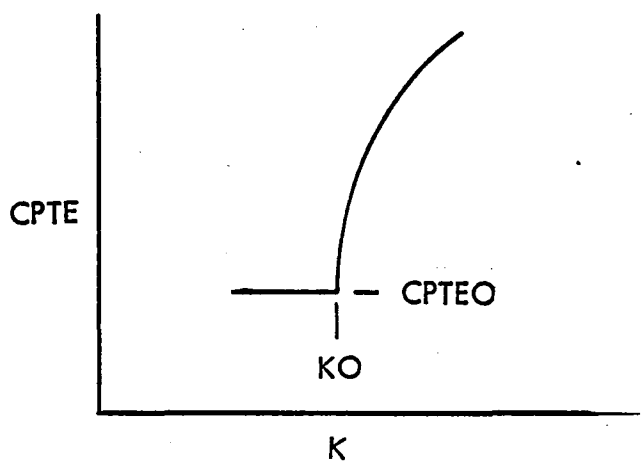

The composite plots showing CPTE - CPTEO plotted against K-KO for the C-141 wing are shown in Figure 14 and are typical of other sets of data which will be presented later. This method of presentation provides an excellent way to judge the entire correlation concept. The "tightness" of the data correlation not only confirms the collapsing of trailing-edge pressure recovery data for angle of attack and Mach number variations, but also demonstrates the invariance of curve shape as Reynolds number is changed. As shown in Figure 14, the quality of the correlation is much improved over that shown in Reference 3. This improvement results partially from deletion of the bubble separation and low speed stall data discussed previously, but also because the unique correlating parameter K collapses the pertinent trailing-edge separation data without the compromise which was inherent in attempting to include the extraneous cases when using the empirical parameter.

The data for the C-141 wing cover a variety of aerodynamic conditions. The inboard station, η = 0.193, is completely free of bubble separation. At the mid station, η = 0.389, approximately 30%, and at the outboard station, η=0.637, 10 to 15 percent of the wind tunnel measured points were deleted because they showed evidence of separation bubbles. Relatively fewer points needed to be deleted from the flight results because the penetration into deep separations was not as great as in the wind tunnel tests. The scatter of data points around the correlation curves is somewhat greater for the two outboard stations than for η = 0.193, but in no case is the scatter great enough that the effect of trailing-edge separation is likely to be significantly misrepresented. The good correlation shown here is rather remarkable when consideration is given to the variety of test data which are included. One test was performed in the PWT 16T tunnel at AEDC using a C-141 wing on a C-5 fuselage covering mean chord Reynolds numbers from about 3 million to 8-1/2 million. The second was obtained from tests of a semi-span wing-fuselage model in the Lockheed-Georgia compressible flow wind tunnel at Reynolds numbers from 3 million to nearly 25 million. The third set was measured in flight tests of the airplane, and lift coefficient and Reynolds number were varied by measuring data at altitudes of 20,000 and 40,000 feet with the airplane in turns or push-overs at load factors from 0 to 2. The airplane was flown into Mach number and load factor conditions where significant buffet was encountered. Because of the large built-in twist of the C-141 wing (5.5°),

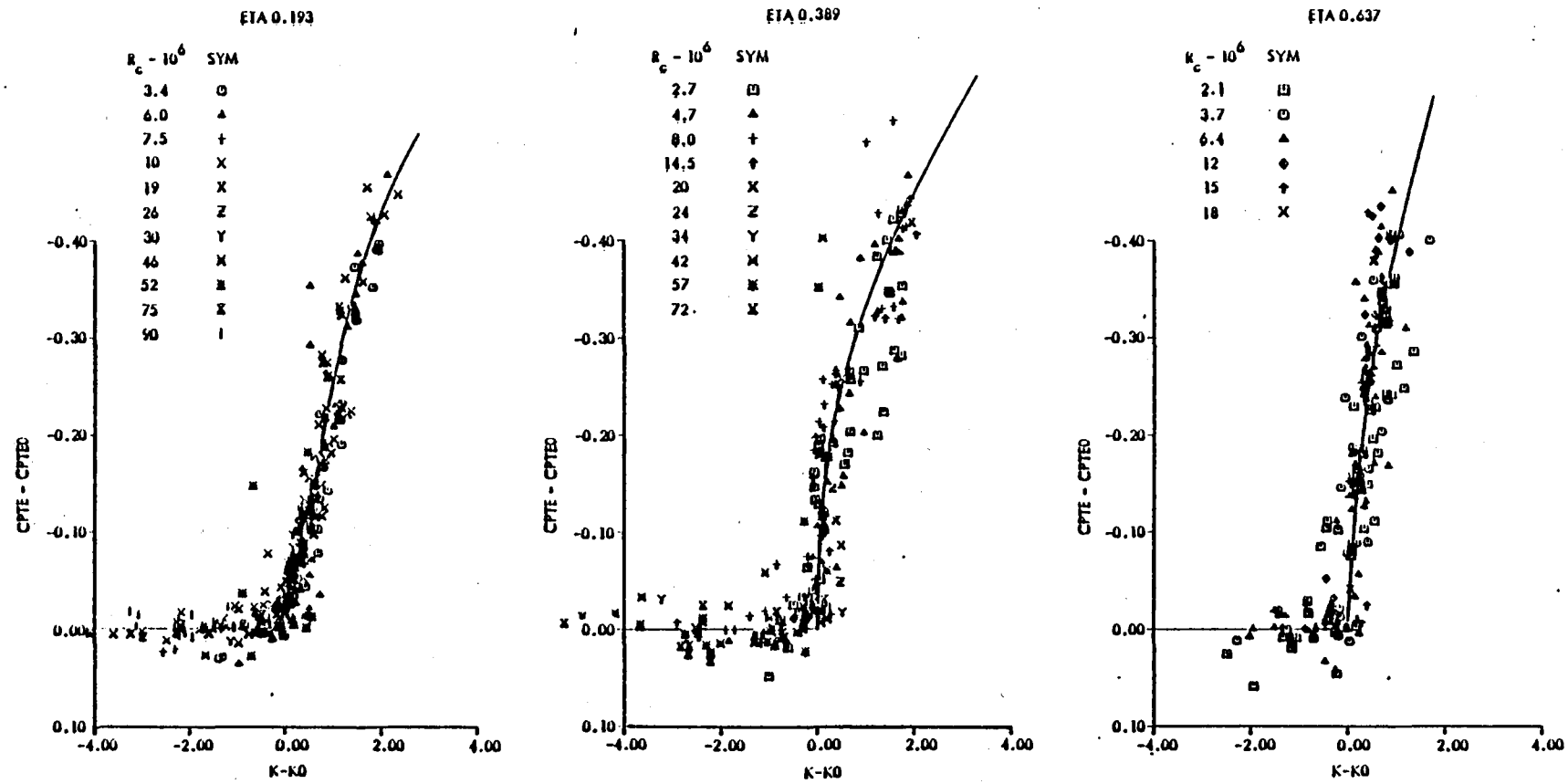

Figure 14. Composite Correlations for C-141 Wing

the farthest outboard station, η = 0.637, very rarely showed any evidence of separation. Although the few points showing degraded trailing-edge pressure recovery were utilized in Reference 3 to establish separation development curves, they have now been abandoned because they are clearly not conclusive.

Pressure distributions were measured at two spanwise stations in both wind tunnel (AEDC 16T) and flight tests of the C-5 airplane. Composite correlations of these data are shown in Figure 15. In this case significant penetration into separated conditions was experienced at both spanwise stations and the available Reynolds numbers range from about 3 million to 90 million. The twist of the C-5 wing is substantially less than the C-141 and conditions are more nearly constant across the span. Approximately 30 percent of the wind tunnel points and 7 percent of flight points have been deleted because of bubble separations.

Data for the RAE model 864 are presented in Figure 16. At the two inboard stations for this wing, data were retained only for the lowest Reynolds number tested. All other data encountered bubble separations and were therefore deleted. At the most outboard station considered, η = 0.793, bubble separations were absent in a sufficient number of cases to enable a complete correlation of data for Reynolds numbers from 3-1/2 to 7-1/2 million. In this case, a large number of data points (approximately 25%) showed characteristics of low-speed stalls and were deleted.

Correlated data for two stations of the wing of the F-8SCW airplane are shown in Figure 17. These data were obtained from Reference 7, which presents the results of flight tests at several Mach numbers quite close to 1. The range of Reynolds numbers covered by these tests is rather limited and no Reynolds number effects are discernable within that range. The characteristic shape of the correlation curves is very much different from that shown by the other wings which have been considered. This is perhaps not surprising in view of the radically different type of wing and the Mach number range covered by these tests. The basic test data (CPTE vs. Mach number and angle of attack) for which these correlations have been developed are shown in Figure 18. The correlating parameter K is successful in collapsing these data into reasonably narrow bands in spite of the large and somewhat disorganized variations which are shown in Figure 18.

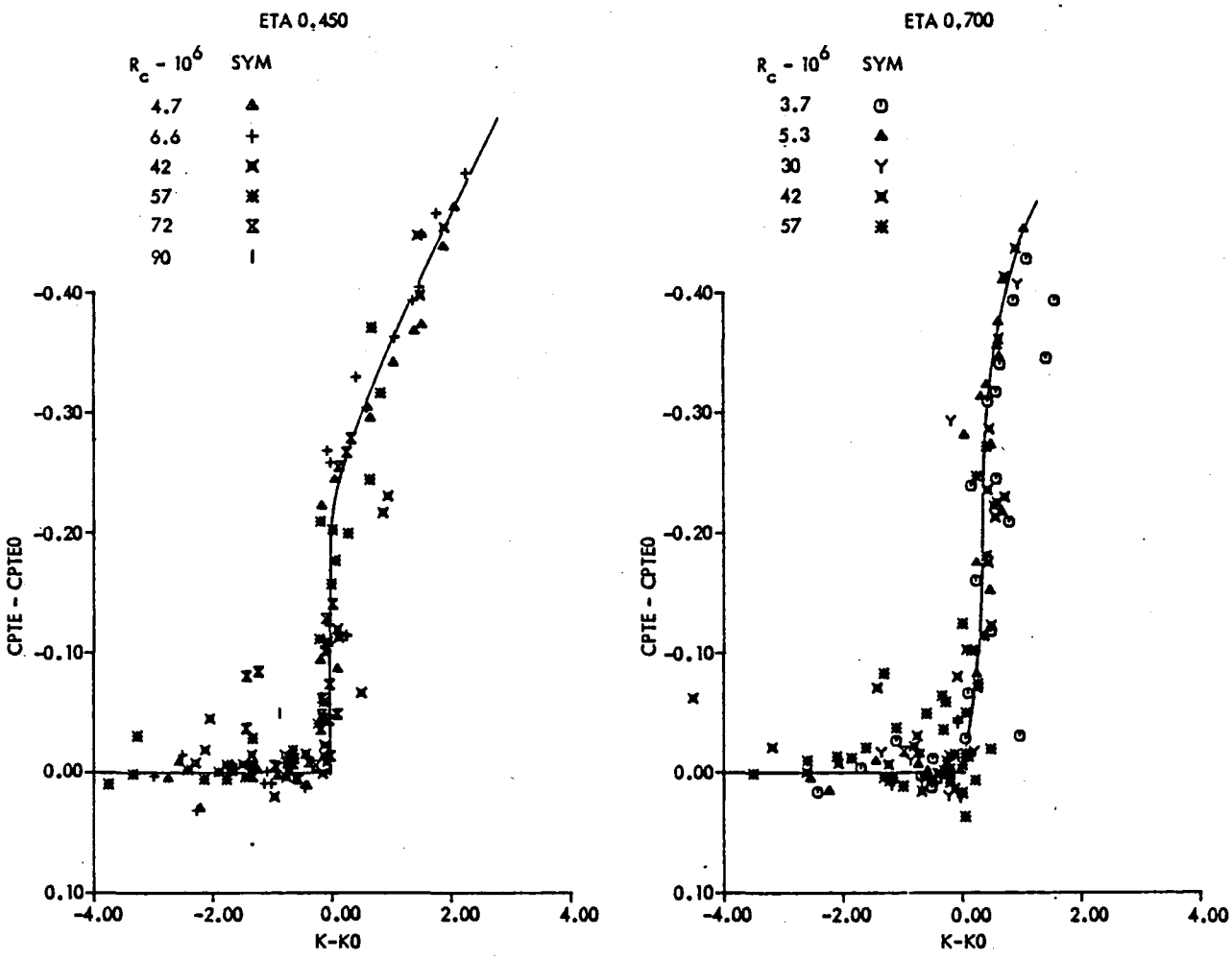

Figure 15. Composite Correlations for C-5 Wing

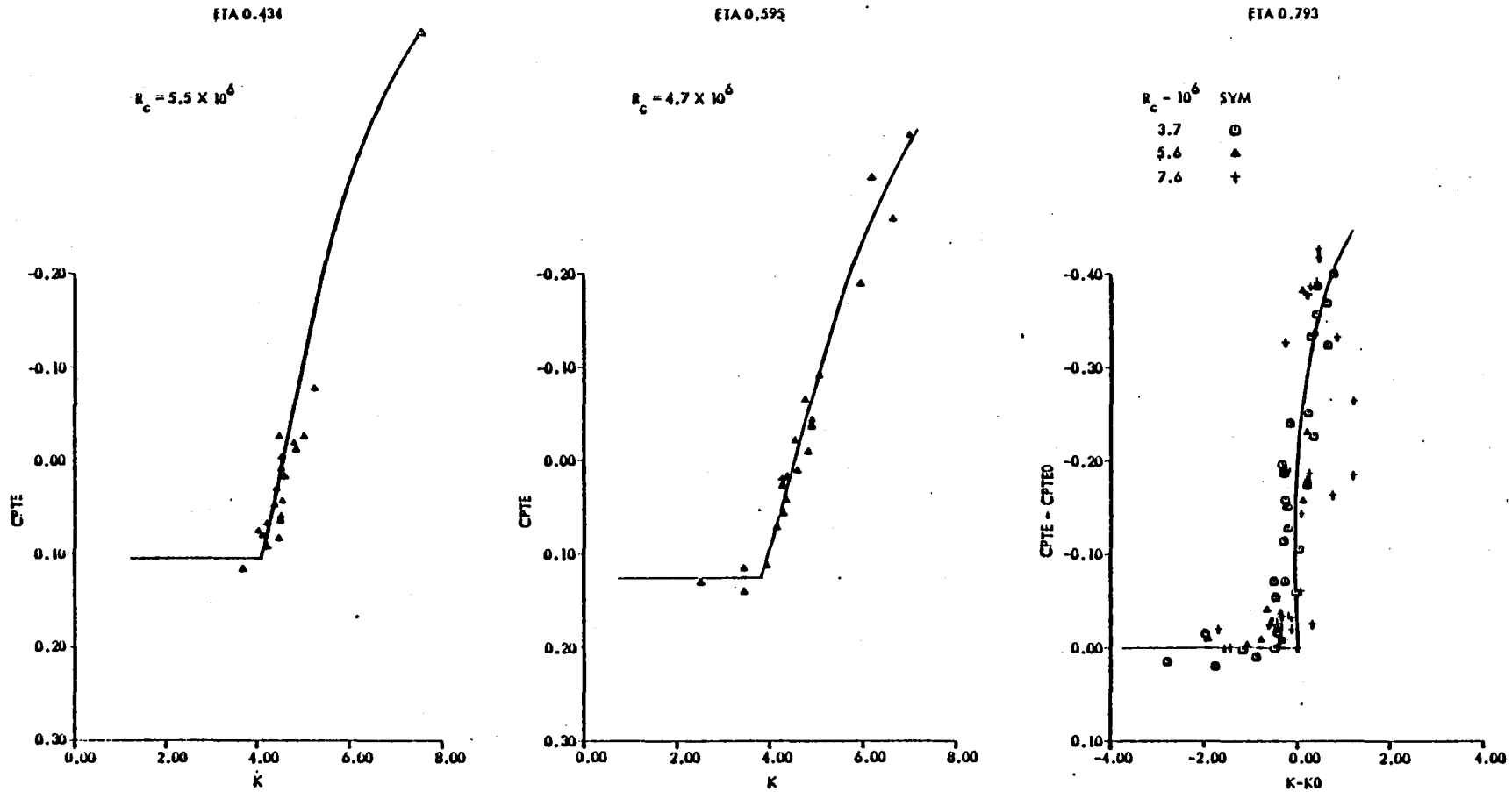

Figure 16. Correlation Data for RAE 864 Wing

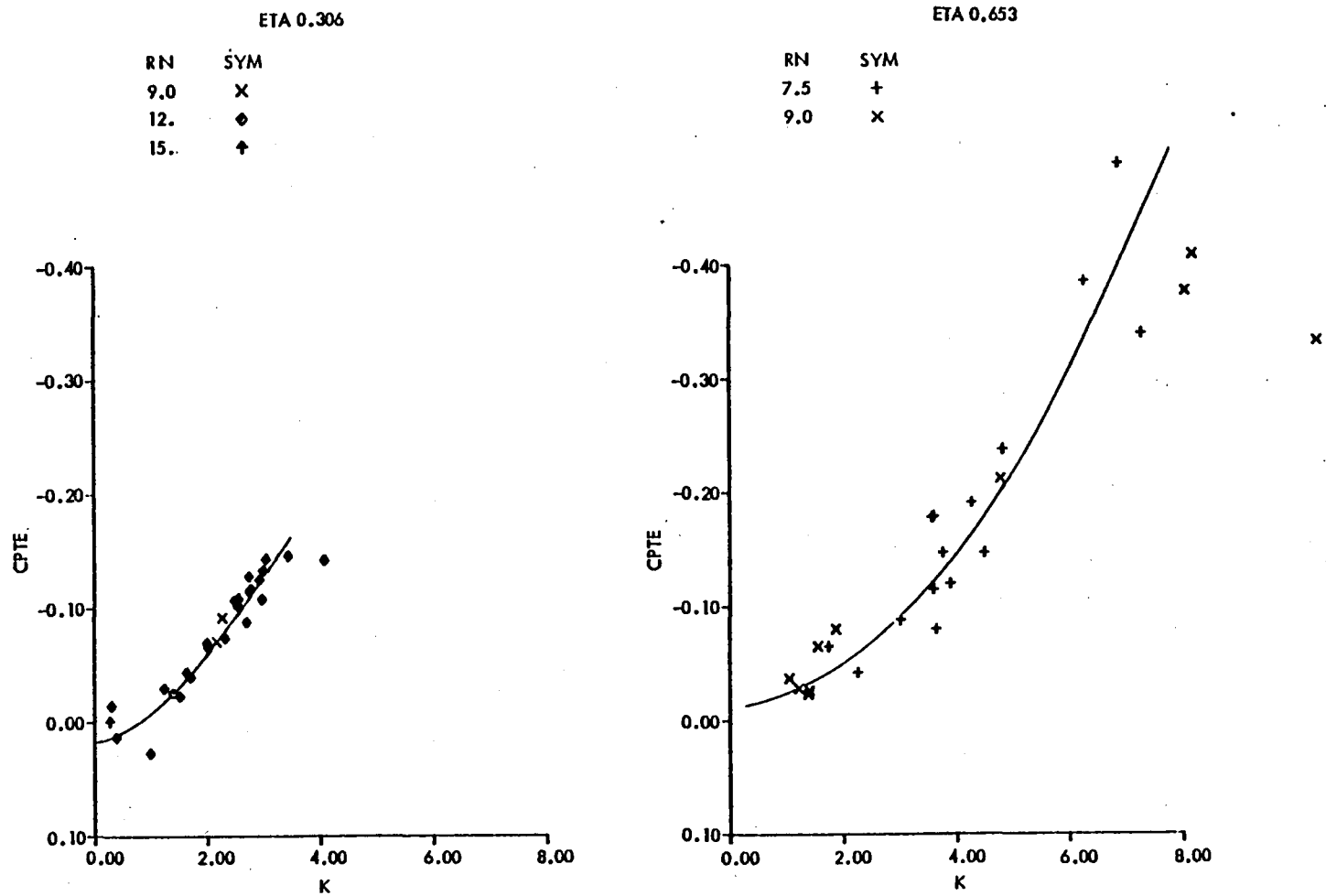

Figure 17. Correlations for F-8 SCW Flight Data

It is wise at this time to point out again (this was previously discussed in Reference 3) the fact that data points selected to calculate the local Mach number M_e in the correlation parameter are those points immediately ahead of the terminal shock, regardless of prior pressure peaks. Pressure distribution plots for several cases are shown in Figure 19 to illustrate this point. The F-8 SCW data are the most striking example. The conditions which enable a successful correlation, and therefore apparently control the development of separation, are those conditions immediately ahead of the shock, even though significantly higher local Mach numbers are encountered farther forward on the wing chord. Those farther forward conditions obviously contribute to the boundary layer development and, therefore, influence separation, but the strength of the terminal shock seems to provide the primary control over separation.

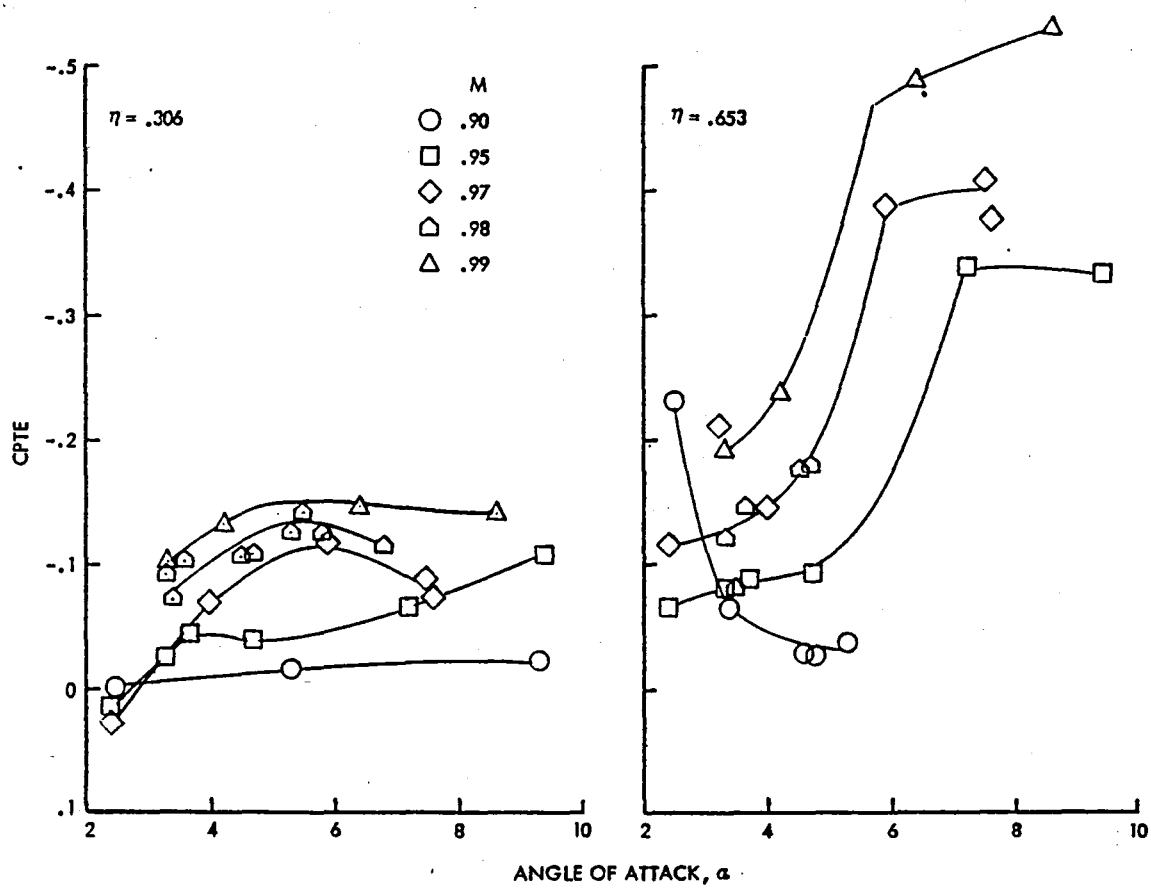

Figure 18. Variation of Trailing Edge Pressure Recovery with Mach Number and Angle of Attack, F8-SCW

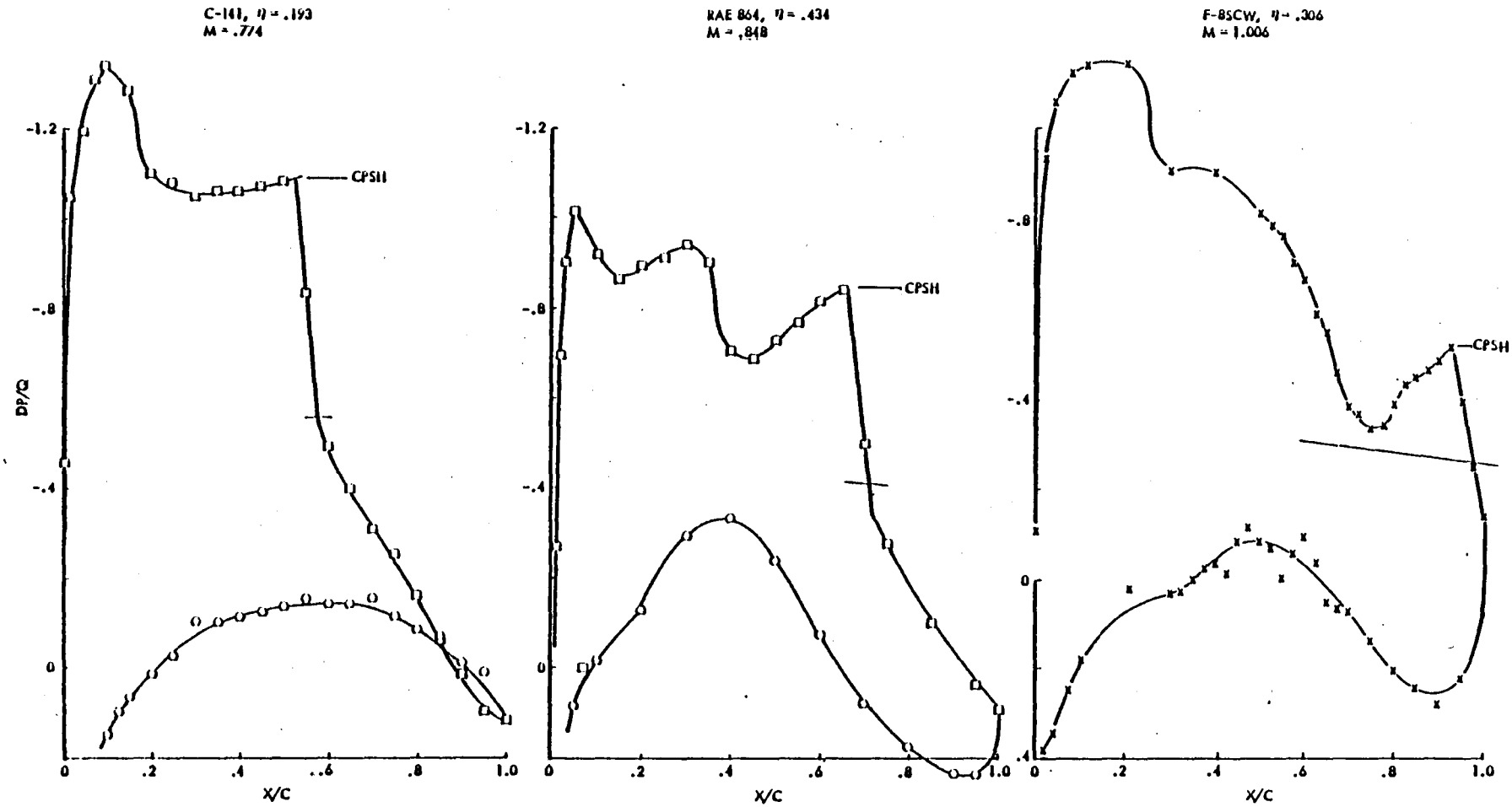

Figure 19. Illustration of Local Flow Conditions used to Define Correlation Parameter

SCALE EFFECTS

A simple observation of the data presented in the previous section shows that Reynolds number effects on the separation development are similar to those shown previously in Reference 3. Quantitatively, however, the Reynolds number effects must be different because the correlation parameter K contains the Reynolds number dependent term C_f. The variations of CPTEO and KO are shown in Figure 20. These data show rather convincingly that the effects of Reynolds number on the separation development (as displayed by the correlation of pressure recovery versus K) is identical for all of the cases considered. These cases include a number of spanwise stations on both the C-141 and the C-5 wings which cover a large Reynolds number range from both wind tunnel and flight test results, and from one spanwise station of the RAE 864 wing. This latter wing includes the primary features of modern supercritical wings including an isentropic recompression ahead of the terminal shock and large pressure gradients in traversing the trailing edge from lower to upper surface.

The close grouping of test data around the faired curves in Figure 20 provides substantial confidence in the applicability of these scale effects to transonic wings in general, although additional cases of combined wind tunnel and flight test results would be desirable for modern transport wing designs.

A review was made of scale effects utilizing R_θ as a scaling parameter rather than R_c. It was thought that refined correlations might be obtained owing to the fact that variations in boundary layer development due to angle of attack changes in pressure distribution are given some accountability in R_θ but not, of course in R_c. No improvement was observed in correlation or scaling. In a similar way, the concept of using the skin friction coefficient itself as a scaling parameter, or of using the calculated value of H just forward of the shock, were examined. None of these showed advantages over the use of chord Reynolds number.

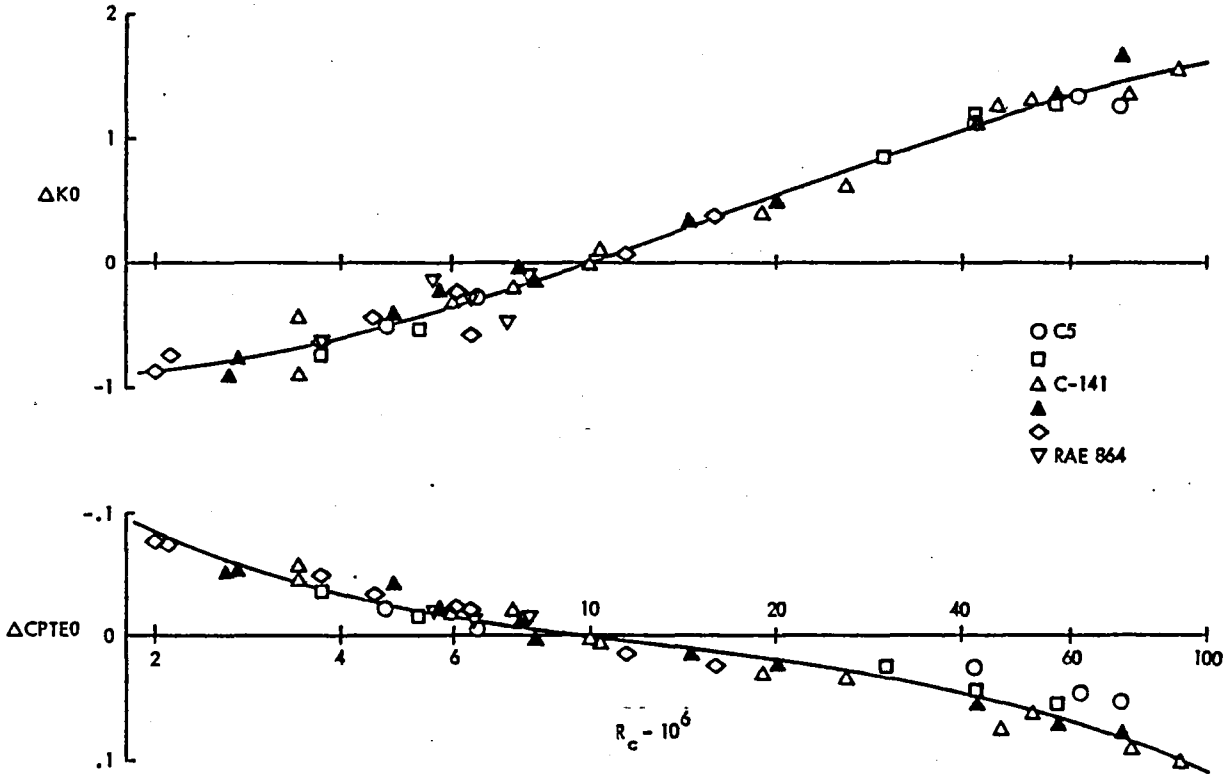

Figure 20. Scale Effect on Shock-Induced Separation Correlations

EXTRAPOLATING PROCEDURE

The procedure for utilizing the concepts discussed in this report for predicting the effect of changes in Reynolds number on wing pressure distributions in the presence of shock-induced trailing-edge separations is discussed in some detail in Reference 3. The principal points of that procedure are listed below and are not changed by the refinements presented in this report:

1. Measure pressure distributions with transition fixed near the leading edge at whatever Reynolds numbers can be achieved in available test facilities. (The impact of precision of the prediction process is of course minimized by starting at the highest possible Reynolds number.) The remaining steps are then undertaken utilizing the measured data at each spanwise station individually.

2. Make plots of shock location, XCSH, against trailing edge pressure coefficient, CPTE for each of the test Mach numbers. The definition of this relationship can be refined by including data measured at additional Reynolds numbers, or with the transition strip removed, or with vortex generators installed on the wing. This relationship is independent of Reynolds number and will be used to define the flight shock location from extrapolated values of CPTE.

3. The values of the correlation parameter K are calculated from measured pressure data and calculated skin friction coefficients. The variation of trailing-edge pressure coefficient with Mach number and angle of attack is collapsed into a single curve of CPTE vs K. Values of CPTEO and KO for the test Reynolds number are picked off that curve.

4. Values of CPTEO and KO for the flight Reynolds number are now obtained by adding increments from Figure 20 to those values for the test Reynolds number. The relationship between CPTE and K for the

flight Reynolds number is produced by shifting the curve from step 3 by those increments.

5. For any given value of K, the values of CPTE and XCSH can be picked off the curves from steps 4 and 2, respectively. The pressure coefficient at the beginning of the shock can be calculated from K, the freestream Mach number, and the appropriate value of C_f. The chordwise location for that pressure coefficient is obtained from shock location and the slope of the shock pressure rise, enabling the definition of a locus of shock initiation points.

Figure 21 illustrates the outcome of this process, using test data at several angles of attack from station $\eta = 0.193$ of the C-141 wing for a chord Reynolds number of 3.4×10^6 and extrapolating to a chord Reynolds number of 100×10^6. The locus of points at which the shock can start for each Reynolds number is shown on the plot for each angle of attack. The fairing of pressure coefficient to the new shock location can be aided by taking guidance from calculated pressure distributions, and the fairings of pressure distributions from the foot of the shock to the trailing-edge is copied from test data experiencing similar trailing-edge pressure recoveries. The test data at an angle of attack of 4° shows the presence of a separation at the foot of the shock and, therefore, requires no scale extrapolation.

The extrapolated pressure distributions are applicable at equivalent angles of attack for the pertinent spanwise station. Proper prediction of spanwise load distributions must take account of the aeroelastic deflection of the wing.

The concepts which underlie this extrapolation procedure show that in general, there is no "magic" Reynolds number beyond which scale effects no longer exist. From a practical point of view however, there is for each Mach number and angle of attack a Reynolds number at which this procedure would predict that these conditions result in a value of K less than the "knee" value at which CPTE begins to deteriorate. At Reynolds numbers above that value, the scale effect on CPTE is reduced to a much smaller rate of change than that for lower Reynolds numbers.

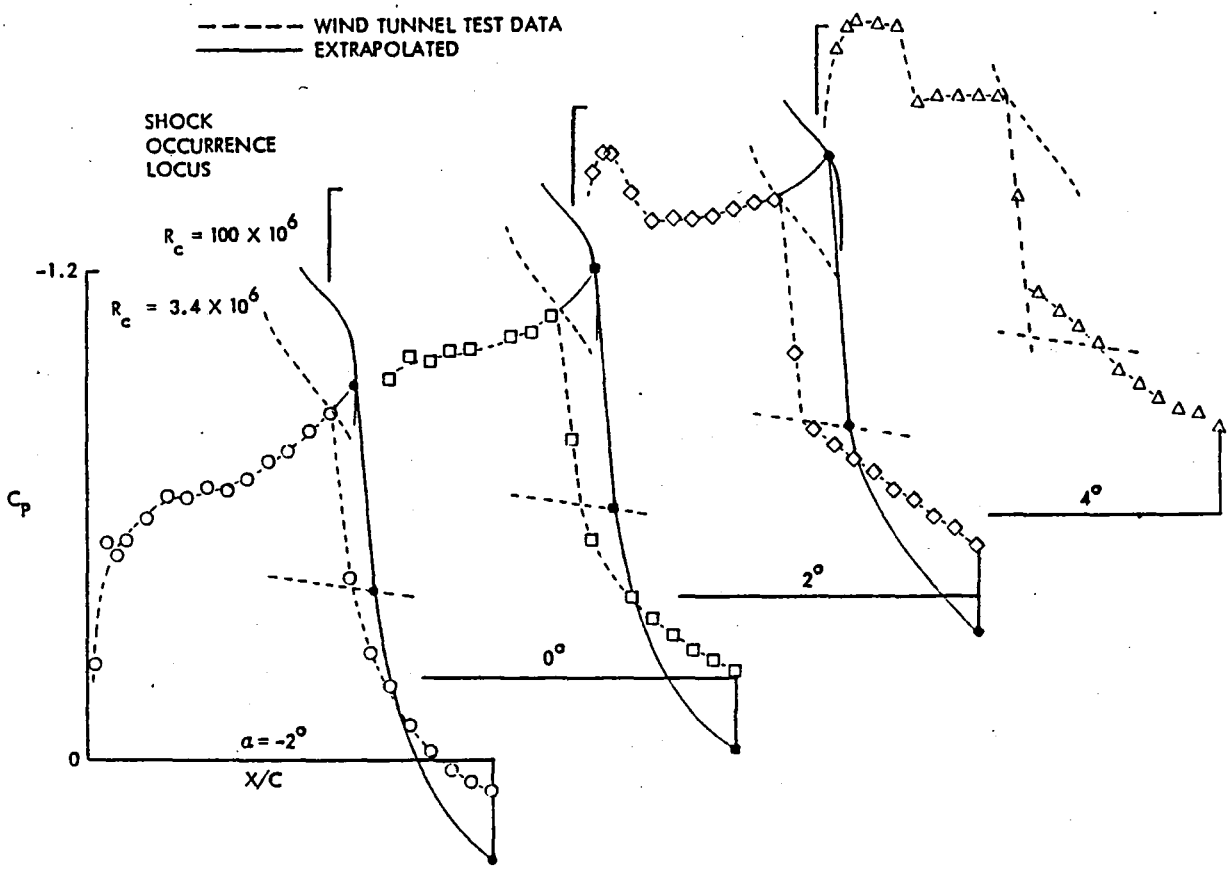

Figure 21. Illustration of Pressure Distribution Extrapolation. C-141, η = .193, M = .825

CONCLUDING REMARKS

The study which is covered by this report was conducted to refine the Reynolds number extrapolation process previously presented in Reference 3, and to exploit the newly derived analytical correlation parameter of Reference 4.

Substantial improvements in the correlation of shock-induced separation data for transonic wings has been demonstrated by use of the analytical parameter rather than the previously used empirical parameter.

A portion of this improvement results from an isolation of data points that are influenced either by local separations at the shock or by phenomena similar to low speed stalls. The presence of either of these factors invalidates the correlation which is directed toward trailing-edge separations.

Specific criteria are not yet known to predict those wings which will experience local separations at the shock. The occurrence of these separations is obviously dependent on Mach number as well as wing geometry. They occur with great frequency at inboard stations of the RAE 864 wing, especially at low Mach numbers; less frequently outboard or at high Mach numbers. They are almost completely absent from inboard stations of the C-141 wing, but occur with moderate frequency farther outboard. It has been shown previously, by other researchers, that flow situations dominated by bubble separations experience no change due to changes in Reynolds number. The fact that these situations are rejected by the current correlation concept is therefore no great loss.

The scale extrapolation process previously presented in Reference 3 is still valid, is possibly somewhat improved in precision, but is quantitatively changed due to the inclusion of skin friction coefficient in the analytical correlation parameter.

REFERENCES

1. Pearcey, H.H., Haines, A. B., and Osborne, J. "The Interaction Between Local Effects at the Shock and Rear Separation" in AGARD Conference Proceedings 35, September 1968.

2. AGARD CP83 "Facilities and Techniques for Aerodynamic Testing at Transonic Speed and High Reynolds Number" April 1971.

3. Cahill, J. F., and Connor, P. C. "Correlation of Data Related to Shock-Induced Trailing-Edge Separation and Extrapolation to Flight Reynolds Number" NASA CR-3178, September 1979.

4. Khan, Mohammad "Analytical Considerations of Shock-Boundary Layer Correlations" NASA CR-166426, Part I, March 1983

5. McNally, William D. "Fortran Program for Calculating Compressible Laminar and Turbulent Boundary Layers in Arbitrary Pressure Gradients" NASA TND-5681 May 1970.

6. Anyiwo, Joshua C., and Bushnell, Dennis M. "Turbulence Amplification in Shock-Wave Boundary-Layer Interaction" AIAA Journal Vol. 20, No. 7, July 1982 P. 893.

7. Montoya, Lawrence C., and Banner, Richard D. "F-8 Supercritical Wing Flight Pressure, Boundary-Layer, and Wake Measurements and Comparisons with Wind Tunnel Data" NASA TMX-3544, June 1977.

End of Document